THM and Reactive Transport Model Development and Evaluation: International Activities

Fuel Cycle Research & Development
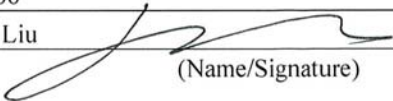
Revision 2
12/20/2012

APPENDIX E

FCT DOCUMENT COVER SHEET [1]

Name/Title of Deliverable/Milestone/Revision No.	THM and Reactive Transport Model Development and Evaluation: International Activities
Work Package Title and Number	DR Generic Engineered Barrier System Evaluations – LBNL FT-13LB080604
Work Package WBS Number	1.02.08.06
Responsible Work Package Manager	Hui-Hai Liu _____ (Name/Signature)

Date Submitted   10/16/2013

Quality Rigor Level for Deliverable/Milestone[2]	☐ QRL-3	☐ QRL-2	☐ QRL-1 ☐ Nuclear Data	☒ Lab/Participant QA Program (no additional FCT QA requirements)

This deliverable was prepared in accordance with   Lawrence Berkeley National Laboratory
_____
(Participant/National Laboratory Name)

QA program which meets the requirements of
☒ DOE Order 414.1   ☐ NQA-1-2000   ☐ Other

This Deliverable was subjected to:

☐ Technical Review   ☐ Peer Review

Technical Review (TR)   **Peer Review (PR)**

Review Documentation Provided   **Review Documentation Provided**

☐ Signed TR Report or,   ☐ Signed PR Report or,
☐ Signed TR Concurrence Sheet or,   ☐ Signed PR Concurrence Sheet or,
☐ Signature of TR Reviewer(s) below   ☐ Signature of PR Reviewer(s) below

Name and Signature of Reviewers

_____   _____

_____   _____

_____   _____

NOTE 1: *Appendix E should be filled out and submitted with the deliverable. Or, if the PICS:NE system permits, completely enter all applicable information in the PICS:NE Deliverable Form. The requirement is to ensure that all applicable information is entered either in the PICS:NE system or by using the FCT Document Cover Sheet.*

NOTE 2: *In some cases there may be a milestone where an item is being fabricated, maintenance is being performed on a facility, or a document is being issued through a formal document control process where it specifically calls out a formal review of the document. In these cases, documentation (e.g.. inspection report, maintenance request, work planning package documentation or the documented review of the issued document through the document control process) of the completion of the activity along with the Document Cover Sheet is sufficient to demonstrate achieving the milestone. If QRL 1, 2, or 3 is not assigned, then the Lab/Participant QA Program (no additional FCT QA requirements box must be checked, and the work is understood to be performed, and any deliverable developed, in conformance with the respective National Laboratory/Participant. DOE- or NNSA-approved QA Program.*

This page is intentionally blank.

CONTENTS

FIGURES

TABLES

ACRONYMS

BBM	Basic Barcelona Model
CIEMAT	Centro de Investigaciones Energéticas, Medioambientales y Tecnológicas
DOE	Department of Energy
EBS	Engineered Barrier System
EDL	Electrical Double Layer
FEPs	Features, Events, and Processes
FLAC	Fast Lagrangian Analysis of Continua
JAEA	Japan Atomic Energy Agency
LBNL	Lawrence Berkeley National Laboratory
THM	Thermal-Hydrological-Mechanical
THMC	Thermal-Hydrological-Mechanical-Chemical
TOUGH	Transport of Unsaturated Groundwater and Heat
UFD	Office of Used Fuel Disposition Research and Development
URL	Underground Research Laboratory

1.   INTRODUCTION

Recognizing the benefits of international collaboration in the common goal of safely and efficiently managing the back end of the nuclear fuel cycle, DOE's Office of Nuclear Energy (NE) and its Office of Used Fuel Disposition Research and Development (UFD) have developed a strategic plan to advance cooperation with international partners (Birkholzer et al., 2013; UFD, 2012). UFD's strategic plan lays out two interdependent areas of international collaboration. The first area is cooperation with the international nuclear community through participation in international organizations, working groups, committees, and expert panels. Such participation typically involves conference and workshop visits, information exchanges, reviews, and training and education. The second area of international collaboration is active R&D participation of U.S. researchers within international projects or programs (UFD, 2012). By active R&D, it is meant here that U.S. researchers work closely together with international scientists on specific R&D projects relevant to both sides. With respect to geologic disposal of radioactive waste, such active collaboration provides direct access to information, data, and expertise on various disposal options and geologic environments that have been collected internationally over the past decades. Many international programs have operating underground research laboratories (URLs) in clay/shale, granite, and salt environments, in which relevant field experiments have been and are being conducted. Depending on the type of collaboration, U.S. researchers can participate in planning, conducting, and interpreting experiments in these URLs, and thereby get early access to field studies without having in situ research facilities in the United States.

UFD considers this second area, active international R&D, to be very beneficial in achieving the program's long-term goals of conducting "experiments to fill data needs and confirm advanced modeling approaches" (by 2015) and of having a "robust modeling and experimental basis for evaluation of multiple disposal system options" (by 2020). Advancing opportunities for active international collaboration with respect to geologic disposal has therefore been the primary focus of UFD's international strategy in the recent year (Birkholzer et al., 2013; Birkholzer, 2012).

Here we report LBNL's international activities related to THM and reactive transport model development. These activities include modeling of field experiments at the Mont Terri URL, Switzerland, and the Horonobe URL, Japan. Sections 2 and 3 below present activities related to respective THM and reactive transport modeling. These activities address key Features, Events and Processes (FEPs), which have been ranked in importance from medium to high, as listed in Tables 7 and 8 of the *Used Fuel Disposition Campaign Disposal Research and Development Roadmap* (FCR&D-USED-2011-000065 REV0) (Nutt, 2011). Specifically, they address FEP 2.2.01, Excavation Disturbed Zone (EDZ) for shale; FEP 2.1.04.01, Buffer/Backfill; FEPs 2.1.07.02, 03, 04, 09, Mechanical Processes; FEPs 2.1.08.03, 07, 08, Hydrologic Processes; and FEP 2.1.11.04, Thermal Processes, by studying coupled processes in the EBS and its interaction with the natural barrier system (a shale formation); and FEPs 2.1.09.52, 53, 54, Chemical Processes—Transport, by investigating reactive-diffusive radionuclide transport in bentonite and/or a shale formation.

2.   MODELING COUPLED THM PROCESSES IN EBS

LBNL is a participating research team in the international DECOVALEX-2015 project. DECOVALEX is a unique international research collaboration, initiated in 1992 for advancing the understanding and mathematical modeling of coupled thermo-hydro-mechanical (THM) and thermo-hydro-mechanical-chemical (THMC) processes in geological systems—subjects of importance for performance assessment of radioactive waste repositories in geological formations. DECOVALEX-2015 is an acronym for the 6th and current phase of the "Development of Coupled Models and their Validation against Experiments" project that is ongoing from 2012 to 2015. In DECOVALEX-2015, LBNL participates in Task B which includes:

Subtask B1) HE-E Heater Test: Studies of bentonite/rock interaction to evaluate sealing and clay barrier performance, in a micro-tunnel at the Mont Terri URL in Switzerland; and

Subtask B2) EBS Experiment: Studies of the thermo-hydro-mechanical-chemical (THMC) behavior of the EBS under heating conditions in both the early resaturation and post-closure stage of the repository and its interaction with the clay host rock, in a vertical emplacement hole at the Horonobe URL in Japan

The model simulations related to these two tasks are carried out using the TOUGH-FLAC simulator (Rutqvist et al., 2002; 2011), which is based on linking the TOUGH2 multiphase flow and heat transport simulator (Pruess et al., 2011) with the FLAC3D geomechanical simulator (Itasca, 2009). The TOUGH-FLAC simulator has been further developed within the UFD campaign and has since been applied to issues related to nuclear waste disposal in clay host rocks, involving bentonite-backfilled emplacement tunnels. As part of this effort, the Barcelona Basic model (BBM) has been implemented for advanced modeling of bentonite backfill behavior (Rutqvist et al., 2013a). The most recent model development involved implementation of a dual-structure model for clay mechanical behavior and an extension to coupled THMC processes related to clay swelling. LBNL is also involved in coupled THM modeling of the Mont Terri URL FE experiment, which is a major large scale field experiment, simulating a full-scale bentonite backfilled repository tunnel. The recent work related to these model developments and modeling of the Mont Terri FE experiment were presented in two recent UFD milestone reports (Davis et al., 2013; Liu et al., 2013).

2.1   Task B1: MONT TERRI URL HE-E HEATER TEST

The Mont Terri URL HE-E Heater Test focuses on THM behavior of bentonite barriers in the early nonisothermal resaturation stage and their THM interaction with Opalinus clay (Figure 2.1). The objective is to better understand the evolution of a disposal system of high level waste in the early post-closure period with emphasis on the thermal evolution, buffer resaturation (*in situ* determination of the thermal conductivity of bentonite and its dependency on saturation), pore water pressure in the near field, and the evolution of swelling pressures in the buffer. Because the test is conducted in a micro-tunnel (at 1:2 scale), it is considered a validation, not a demonstration experiment. The heating test involves two types of bentonite buffer materials (Figure 2.1, left). The heater-buffer interface is heated to a maximum temperature of 135°C and a temperature of 60–70°C is expected at the buffer-rock interface. A dense instrumentation network was in place in the host rock surrounding the micro-tunnel from a previous experiment testing the impact of ventilation on the clay host rock and has been improved for the purpose of the HE-E Heater Test (up to 40 piezometers in total); various sensors have also been placed in the buffer material. The heating phase has started in late summer of 2011 and is being continued for at least three years.
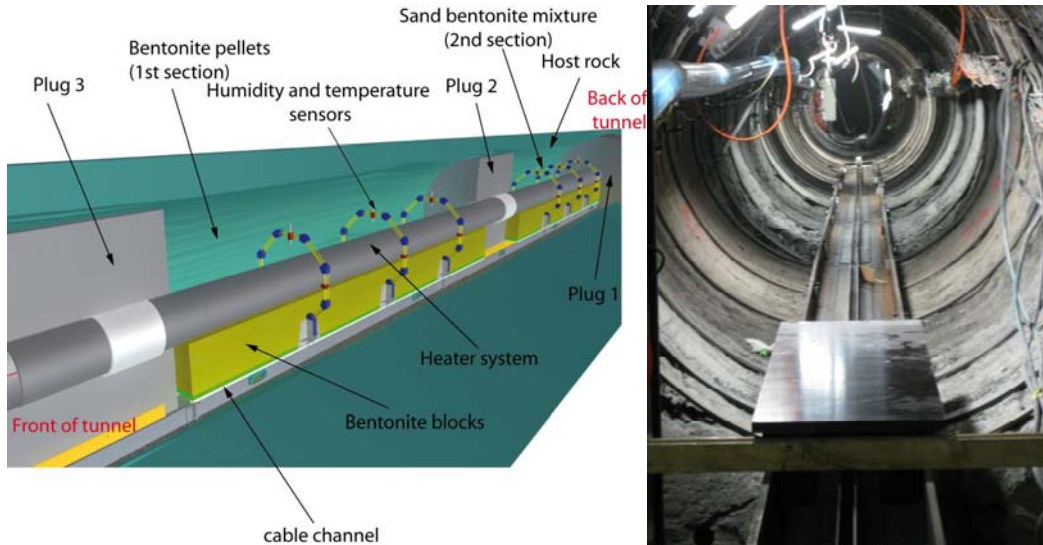
Figure 2.1. Schematic setup of HE-E heater test at Mont Terri and photo of micro-tunnel (Garritte, 2012).

In DECOVALEX-2015 (Task B1), eight international research teams are participating in the modeling of the HE-E experiment. Task B1, which is running over 3 years, is divided into the following steps:

- Step 1a: Opalinus clay study including HE-D experiment, literature study, processes understanding and parameter determination.

- Step 1b: Buffer material study including CIEMAT column cells, literature study, processes understanding and parameter determination.

- Step 2: HE-E predictive modeling using as-built characteristics and true power load. Modeling is 2D (axisymmetric, plane strain or combination) and 3D.

- Step 3: HE-E interpretative modeling when data are made available.

Step 1a started in 2012 with the modeling of the previous HE-D experiment for in situ characterization of THM material parameters for the Opalinus Clay. The DECOVALEX-2015 project is currently in Step 1b, which is a study of buffer material properties through modeling of laboratory experiments on buffer material samples. The buffer material study is mainly focused on modeling and analysis of a THM column experiment conducted by CIEMAT, Spain.

In the following subsections, we present the results of the modeling of the HE-D experiment and the current status on the modeling of CIEMAT column experiment.

2.1.1   Modeling of the HE-D Experiment

The HE-D experiment was conducted between March 2004 and June 2005 by *in situ* heating of Opalinus Clay from two heaters placed in a horizontal borehole (Figure 2.2) (Wileveau, 2005; Gens et al., 2007). Around this heating borehole, about 30 temperature sensors, 10 water pressure sensors, and 3 extensometers were placed, which allowed for monitoring the evolution of the variables induced by the heating (Wileveau, 2005; Gens et al., 2007). Approximately one month after installation, the heaters were switched on with a total power of 650 W (325 W per heater). The heaters were then left under constant

power for 90 days. Afterwards, the power was increased threefold, to 1950 W (975 W per heater), and maintained at that level for a further 248 days. At the end of this second heating stage, the heaters were switched off and the clay was allowed to cool down. Temperature, pore pressure, and deformation were measured throughout. In Figure 2.2, the positions of the main temperature and pore pressure sensors with respect to the heater axis are indicated.
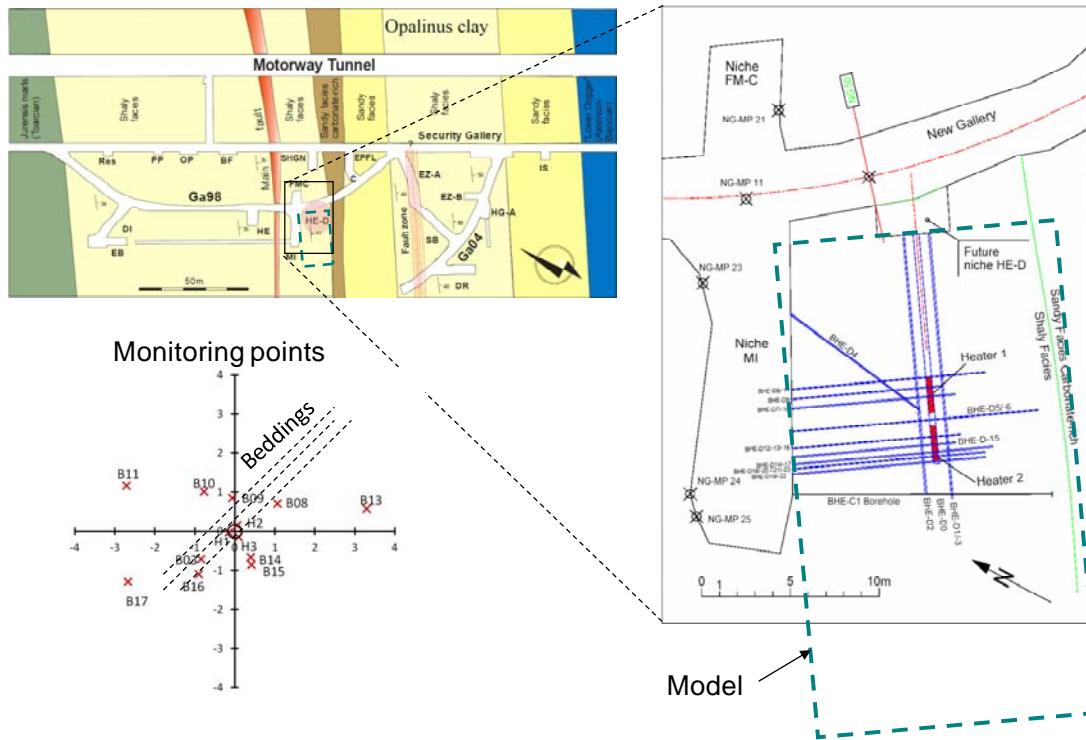
Figure 2.2. Layout of the HE-D experiment including (a) location in the Mont Terri URL, (b) monitoring points, and (c) top view of experiment including monitoring borehole layout (Wileveau, 2005; Rutqvist et al., 2013b).

2.1.1.1   Model Setup

The key of the HE-D modeling is to accurately represent the anisotropic THM behaviour of the Opalinus Clay when it is heated. Opalinus Clay is an argillaceous rock sedimented in marine conditions (Middle Jurassic) with sedimentation planes that results in anisotropic properties. Typical properties of the Opalinus clay are a low permeability of approximately 5×10^{-20} m^2, a porosity of 0.16 and a bulk density of approximately 2450 kg m^{-3} (Wileveau and Rothfuchs, 2007). The mechanical properties of Opalinus clay is usually described as a transversely isotropic elastoplastic material. The heat conductivity tensor can also be considered as transversely isotropic (Garitte et al., 2013).

We modeled the HE-D experiment using the TOUGH-FLAC simulator employing an anisotropic material model considering the beddings of the Opalinus Clay. To accurately model anisotropic thermal and hydrological behavior in TOUGH2, the mesh is inclined along with the beddings. Anisotropic mechanical material behavior is simulated using a so-called ubiquitous joint model, available in FLAC3D, with properties derived from published work (Corkum and Martin, 2007).

We constructed a 3D TOUGH-FLAC model involving a 45° inclined mesh as shown in Figure 2.3. The model dimensions (16×16×28 m) are equivalent to those used by Gens et al. (2007) in their modeling of the HE-D experiment. We used the thermal heat load according to the electric power supplied, and conducted sensitivity studies to back-calculate the *in situ* THM properties of the Opalinus Clay. The rock mechanical properties for the Opalinus Clay were taken from Corkum and Martin (2007). These included parameters for the FLAC3D ubiquitous joint model defining anisotropic strength properties, a bulk modulus of 4.17 GPa, and a shear modulus 1.92 GPa. The thermal expansion coefficient was set to $1.4×10^{-5}$ °C^{-1} which is a representative isotropic average value of the Opalinus Clay (Gens et al., 2007). Finally, we assigned an isotropic permeability of $5×10^{-20}$ m^2, and pore compressibility of $1×10^{-9}$ Pa^{-1}, based on Gens et al. (2007). In the simulation presented here the permeability was set to an isotropic value $5×10^{-20}$ m^2 according to previous simulations by Gens et al. (2007), although permeability at the Mont Terri is anisotropic by a factor of about 4.

Inclined mesh for best representation of thermal anisotropy in the TOUGH2 simulator
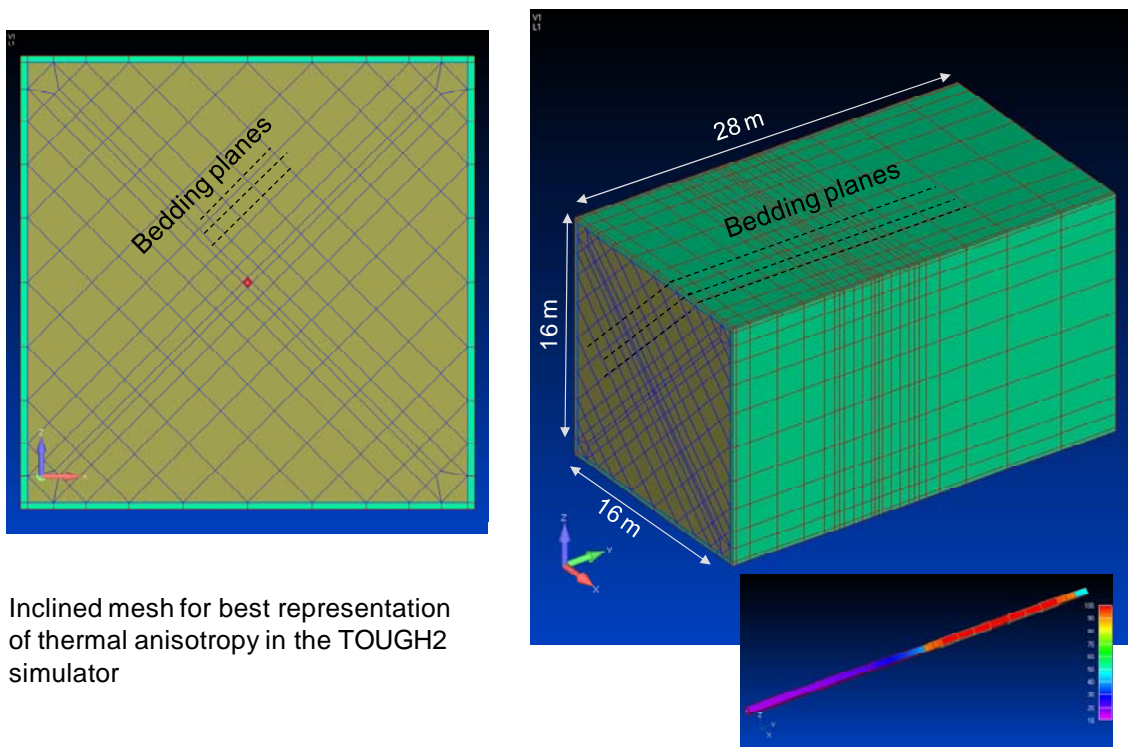
Figure 2.3. TOUGH-FLAC model for the analysis of coupled THM processes at the HE-D experiment.

The initial hydraulic and thermal conditions for the model simulation were 2 MPa in pore fluid pressure and 15°C in temperature within the host rock. The 2 MPa of pore pressure is not under hydrostatic conditions, and the process is affected by the existing tunnel system at the site. A stress field was applied based on the best estimated Mont Terri *in situ* stresses. The vertical stress was set to 7 MPa, whereas the maximum and minimum horizontal stresses were respectively set to 5 MPa and 2 MPa (parallel beddings).

2.1.1.2   *Results with Comparison to Field Data*

The modeling shows that the heating of the rock mass is the driving force for the THM responses in the HE-D experiment. Temperature changes strongly affect hydraulic and mechanical responses whereas thermal processes are not significantly impacted by the hydraulic and mechanical processes. Heat transfer is dominated by thermal conduction and the temperature evolution can be calculated independently of the hydraulic and mechanical processes. In this case we input the heat load as shown in Figure 2.4 and then calibrated the transversely anisotropic thermal conductivity until a good agreement was obtained between simulated and measured temperature evolution at 31 locations in the rock mass. A good overall temperature match was obtained for thermal conductivity parallel to the bedding planes, $K_{\parallel} = 2.15$ W/m-K, and perpendicular to bedding planes, $K_{\perp} = 1.19$ W/m-K; a thermal conductivity anisotropy factor, $K_{\parallel}/K_{\perp} = 1.8$. Figure 2.5 shows the simulated and measured temperature evolution near the heaters and the heat loss along the heater borehole towards niche HE-D. Moreover, an additional heating-system power loss of 5% was assumed for achieving the best overall match between simulated and measured temperature evolution.
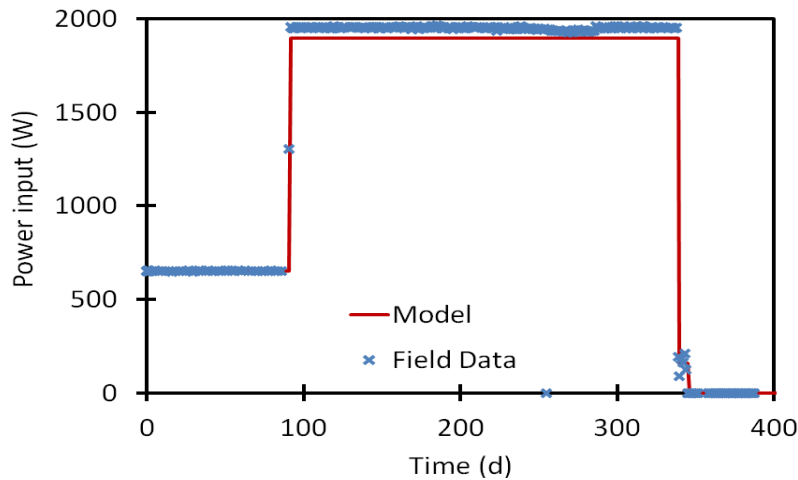
Figure 2.4. Modeled and measured power input for the HE-D experiment.
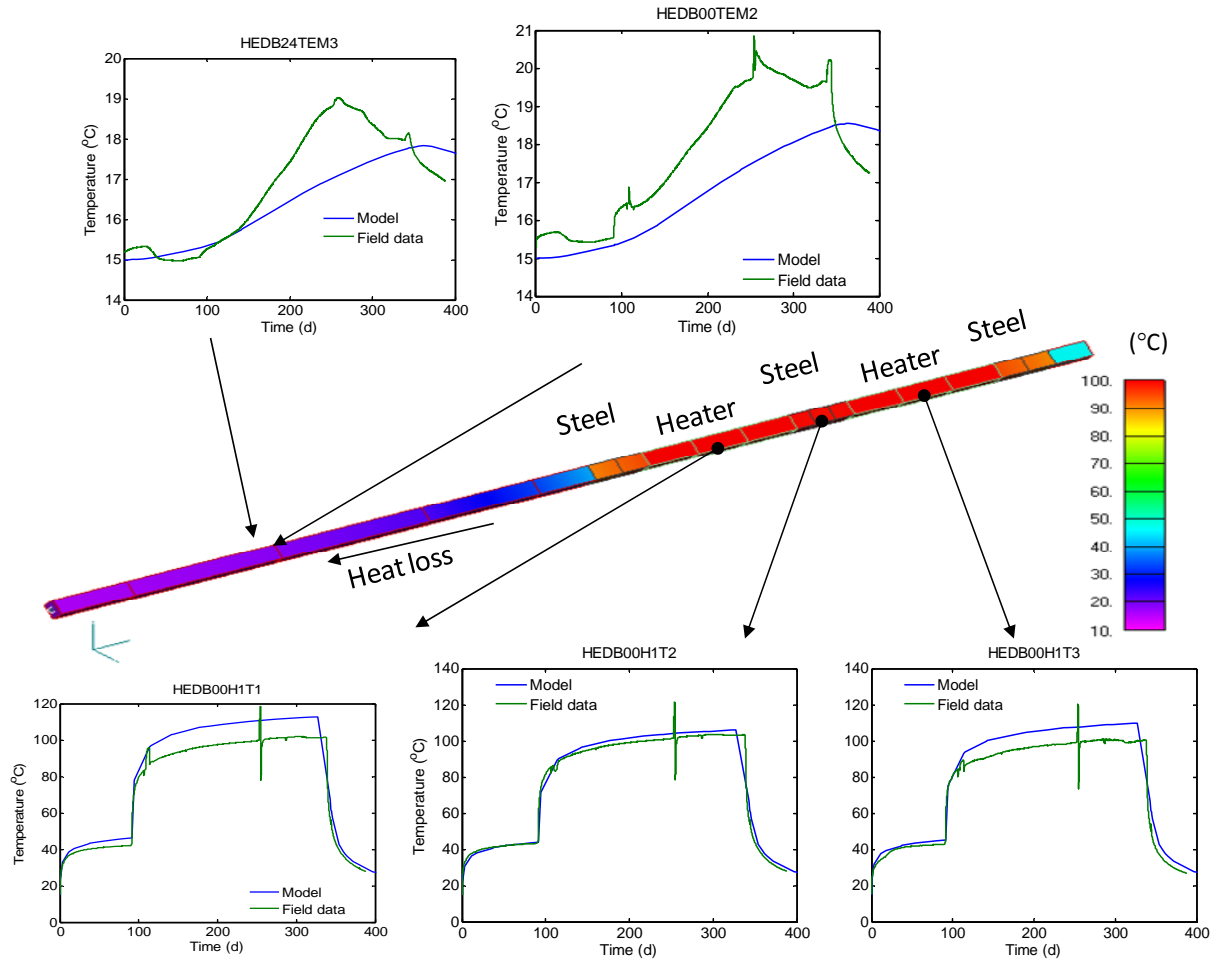
Figure 2.5. Simulated and measured temperature evolution near the heaters and heat loss along equipment in the boreholes toward niche HE-D.

Figure 2.6 presents 3D contour plots of temperature, volumetric strain and pressure after 300 days of heating. The figure shows that rock volumetric strain is up to 0.1% near the heaters whereas the fluid pressure increases to about 3.8 MPa. The change in temperature has a direct impact on the volumetric strain through thermal expansion. Considering free thermal expansion, the volumetric strain caused by a temperature increase from 15 to 50°C is expected to result in a maximum thermal expansion of $\Delta\varepsilon_V = 3\times\Delta T\times\alpha_T = 3\times35\times1.4\times10^{-5} = 0.0015$, or 0.15%. In this case the thermal expansion is not free and some thermal strain will be taken up by the confined rock mass as thermal stress. The thermal expansion of the fluid inside the pores is the cause of increasing fluid pressure, so-called thermal pressurization. Such a pressure increase might also result in additional volumetric strain. However, considering a simple analytic calculation we could estimate this for free strain from the pressure change ΔP and bulk modulus K as $\Delta\varepsilon_V = \alpha_{biot} \times \Delta P/K = 0.6 \times 2\times10^{6}/ 4\times10^{9} = 0.0003$, or 0.03%. Thus, the volumetric strain is mainly thermal strain.

(a)

(b)

(c)
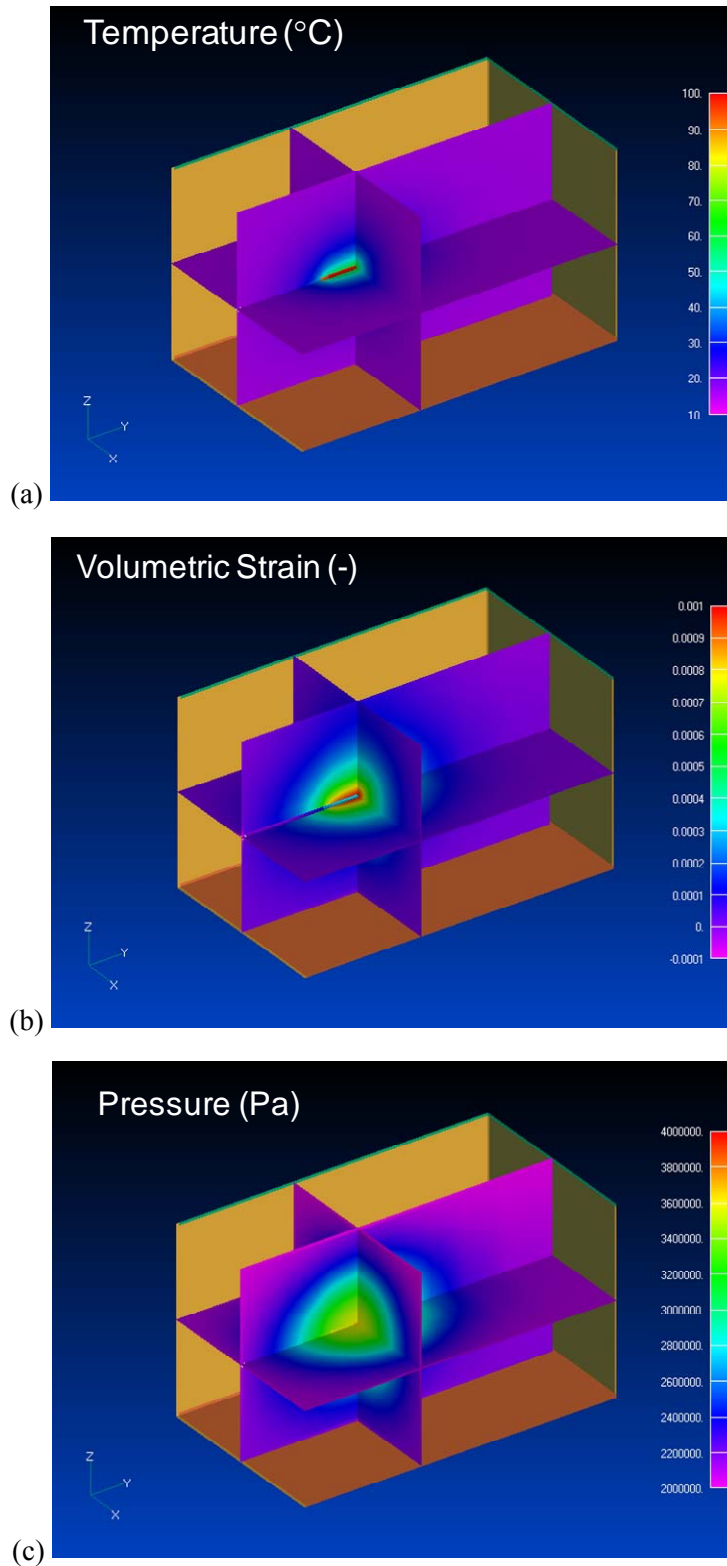
Figure 2.6. Simulated contours of (a) temperature, (b) volumetric strain and (c) pressure after 300 days of heating.

Figure 2.7 shows comparison of simulated and measured temperature and pressure at two monitoring points (B16 and B15), and strain at another location. The simulation shows a correlation between temperature and fluid pressure as a result of thermal pressurization, which occurs as a result of the differences in the coefficient of thermal expansion between the fluid and the solid rock. As previously mentioned, a good temperature agreement is achieved using an anisotropic thermal conductivity. A reasonably good agreement between simulated and measured pressure is achieved with the permeability set to 5×10^{-20} m^2 and a pore compressibility of 1×10^{-9} Pa^{-1}. This pore compressibility was estimated from the elastic properties of the rock assuming uniaxial strain conditions (Rutqvist et al., 2013a). The strain results shown in Figure 2.7 were measured from the relative displacement between two anchor points located about 1 m from each other and in the radial direction from the heater hole. The fact that these anchor points are located in the radial direction means that radial strain can be back calculated from the relative displacements between these anchor points. The radial strain mainly shows a compression during heating as rock is expanded from the heated borehole.
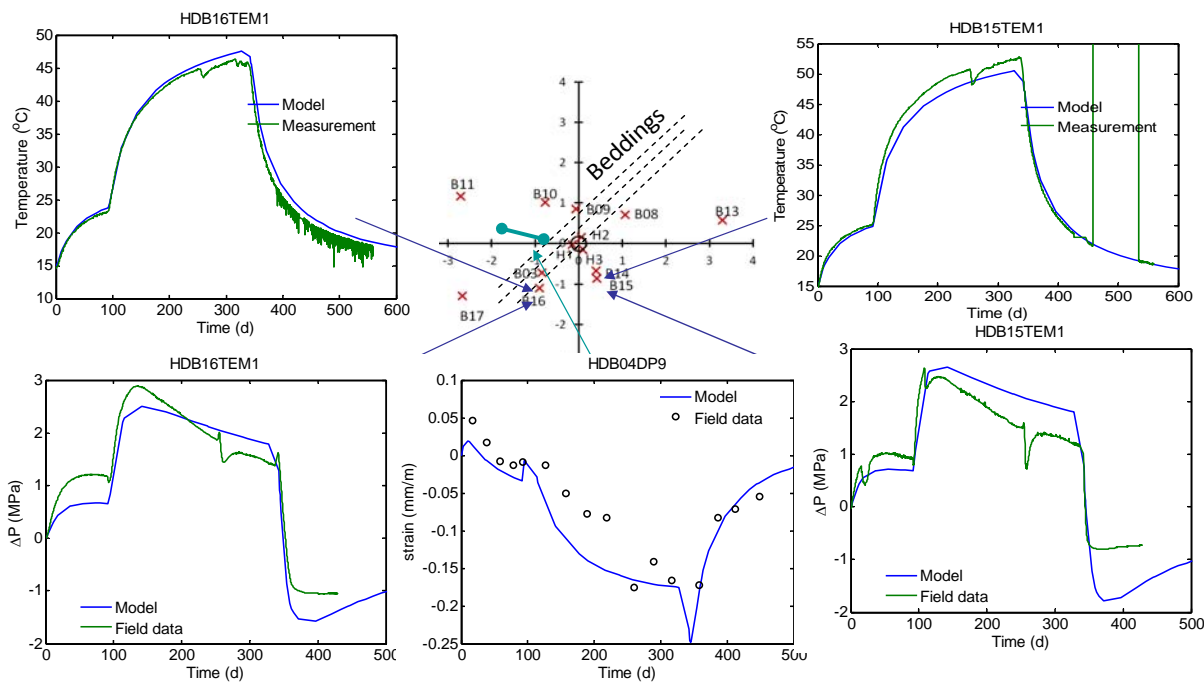
Figure 2.7. Comparison of simulated and measured temperature and pressure at two monitoring points (B15 and B16) and stain at another location close to the heater.

As previously mentioned, a total of eight modeling teams are involved in comparative calculations of the THM processes with different codes (Table 2.1). The comparison of the results for the temperature field shows a good agreement between the teams and the simulated temperatures are close to the measurements. One example is shown in Figure 2.8 for two temperature sensors. Sensor HEDB03 is located at a distance of 1.11 m away from the centre of the heater parallel to bedding, whereas sensor HEDB14 is located 0.775 m away perpendicular to bedding. Figure 2.8 shows a good agreement between the results of the different groups as well as between simulations and observations. The comparison of these sensors also illustrates the effect of the anisotropic heat conductivity of Opalinus clay. Despite the different distance to the heater, both sensors show a similar course of temperature evolution over time. The largest disagreement shown is for one team at sensor HEDB14 in which the temperature was

overestimated because the simulation was conducted with an axisymmetric model in which the thermal anisotropy could not be considered. The modelling of the HE-D heater test is now completed and detailed comparison of the simulation results of different research teams are underway within the DECOVALEX-2015 project.

Table 2.1. Modeling teams participating in Task B1 of DECOVALEX-2015 Graupner et al., 2013)

Team	Principal Investigator	F.O.	Country	Code	2D/ 3D	T-H-M	Heater
UFZ	W. Wang	BGR	Germany	OpenGeoSys	3D	THM	int.
CAS	P. Pan	CAS	China	EPCA3D	3D	THM	Bc
LBNL	J. Rutqvist	DOE	USA	TOUGH-FLAC	3D	THM	int.
ENSI	B. Graupner	ENSI	Switzer-land	OpenGeoSys	3D	THM	int.
	S.T. Nguyen	IRSN	Canada/France	COMSOL	3D	THM	Bc
JAEA	S. Nakama	JAEA	Japan	THAMES	3D	THM	Bc
KAERI	C. Lee	KAERI	South Korea	FLAC3D	3D	THM	int.
CNWRA	C. Manepally	NRC	USA	FLAC-xFlo	2D	TH(M)	Bc
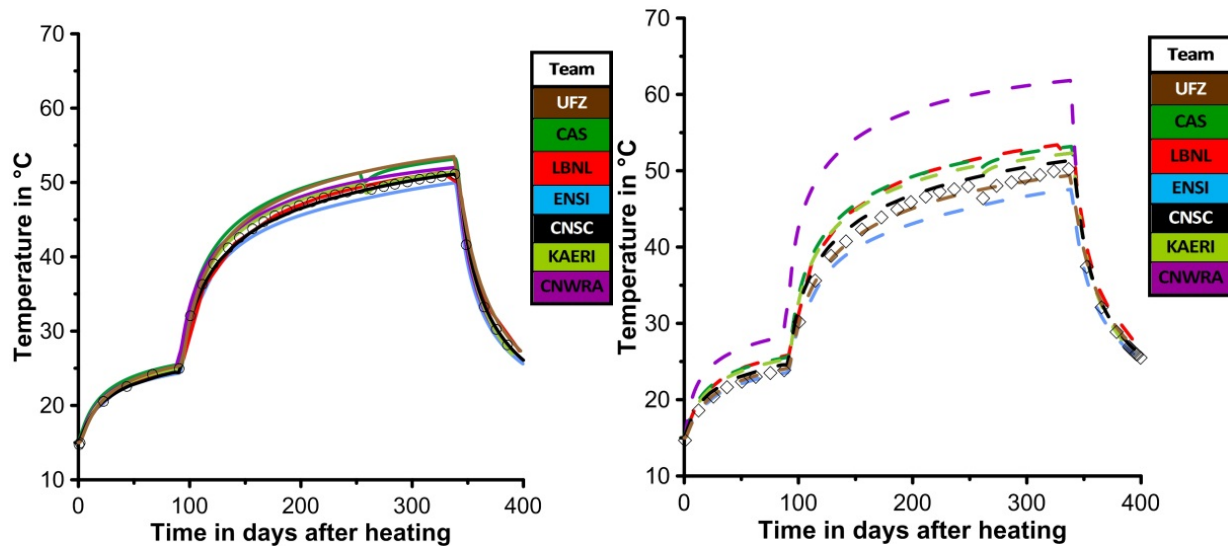
Figure 2.8. Comparison of measurements and model results of for the temperature evolution over time at sensors HEDB03 and HEDB14 (Graupner et al., 2013).

2.1.2   Buffer Material Study

The buffer material study within the DECOVALEX-2015 Task B1 mainly consists of modeling a column experiment on granular MX-80 bentonite. The experiment was conducted in a closed system where the bottom was heated to a high temperature and the top was kept at ambient temperature. Temperature and relative humidity at three points along the axis of the column were measured over time. The objective of this study is to calibrate the water retention curve, the dependency of thermal conductivity on water saturation, and the dependency of water relative permeability on degree of saturation against the relative humidity and temperature data measured in a laboratory column experiment. The model simulations reported here were conducted with the inverse modeling and optimization tool iTOUGH2 (Finsterle, 2007).

2.1.2.1   Description of the Column Experiment

Bentonite pellets were poured into the Teflon column without extra packing. The Teflon column was initially wrapped with a layer of foam, the insulation layer was later replaced with wool. A heater was placed at the bottom of the column and the temperature of the heater was controlled by adjusting the power input using a digital relay. At the top of the column was a cooler where water was circulated through the inner channels of the cooler to maintain the temperature to be the ambient temperature. Sensors were installed with distances of 10 cm, 22 cm, and 40 cm from the heater. Temperature and relative humidity were measured during the experiment.
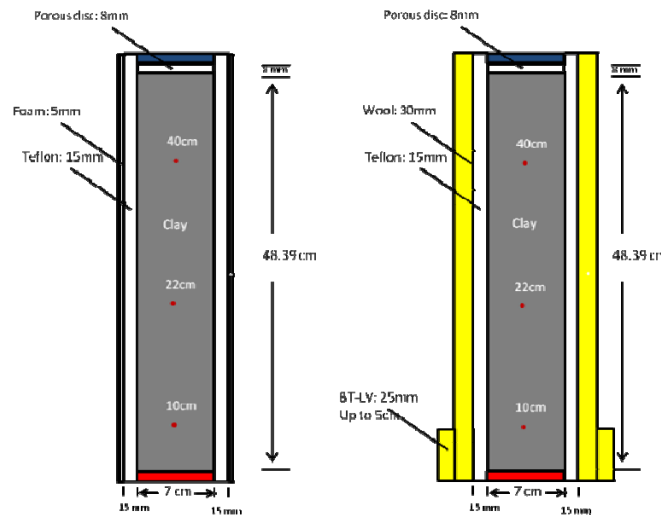
Figure 2.9. Schematic of experimental setups before and after changing insulation.

After the system was assembled, the data acquisition system was turned on and measured the relative humidity and temperature for 140 hours without heating the system. The measured results showed that the relative humidity is quite uniform along the column (~40%). The heater was turned on at t=0. After heating for 33 minutes, the temperature of the heater increased to the target temperature of 100 ºC. The temperature of the heater was then maintained at 100 ºC while the temperature of the cooler was kept at 21.5 ºC. After 1566 hours, the foam layer was replaced with wool of 30 mm thickness covering the entire column length and BT-LV of 25 mm thickness covering the bottom 5 cm. After 3527 hours, the target temperature of the heater was adjusted to 140 ºC. The temperature increased to 140 ºC 17 minutes after the adjustment was made. The experiment was stopped after 5015 hours.

2.1.2.2 Model Development

A 2D radial symmetric mesh was created to simulate the column experiment. The mesh has 6 columns and 28 rows (Figure 2.10). Materials used in the model include Bentonite pellets (BENTL), porous disk (PORUS), heater (HEATR), cooler (COOLR), Teflon (TEFLN), foam (FOAMA), wool (WOOLA), BT-LV insulation (BTLVA), and air (AIRLT). The Bentonite pellets are represented by a column of elements (1×25 elements). Other elements represent the porous disk, heater, cooler, insulation materials, and air.

The bentonite properties used in the model are as shown Table 2.2. The bentonite pellets have a solid grain density of 2700 kg/m^3, intrinsic permeability of 3.5×10^{-21} m^2, and porosity of 0.46. The thermal conductivity of bentonite is 1 W/m-K when saturated with water, in contrast to 0.3 W/m-K under dry conditions. The specific heat of the bentonite pellets is 950 J/kg-K. Before the experiment started, the pores of the bentonite pellets were initially saturated with 22% of water and the measured relative humidity was uniformly 40% along the column.

Table 2.2. Properties of Bentonite pellets used in the model

Solid grain density	2700 kg/m^3
Porosity	0.46
Intrinsic permeability	3.5×10^{-21} m^2
Saturated thermal conductivity	1 W/m-K
Unsaturated thermal conductivity	0.3 W/m-K
Specific heat	950 J/kg-K
Tortuosity	0.67

From laboratory experiments it has been observed that the gas permeability in unsaturated bentonite is about six orders of magnitude higher than the liquid permeability under saturated conditions (Olivella and Gens, 2000). To account for the increased gas permeability, we consider vapor and air diffusion and Klinkenberg effect in the model. A diffusion coefficient of 2.13×10^5 m^2/s is used for both components and a tortuosity of 0.67 is used in the model. A Klinkenberg parameter of 2.5×10^{11} Pa is used.

We use the van Genuchten formula to describe the water retention curve (van Genuchten, 1980).

$$P_c = -P_0\left[(s^*)^{-1/\lambda} - 1\right]^{(1-\lambda)} \tag{2.1}$$

$$s^* = \frac{(s_l - s_{lr})}{(s_{ls} - s_{lr})} \tag{2.2}$$

with the parameters given in Table 2.3.

Table 2.3. Capillary pressure of Bentonite pellets used in the model

λ	0.512
s_{lr}	0
$1/P_0$ (1/Pa)	3.5E-08
P_{max} (Pa)	3×10^9
s_{ls}	1.0
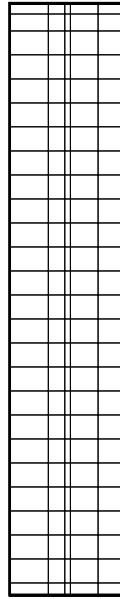
Figure 2.10. Model mesh of the column experiment.

A power law function is used to describe the relative permeability of liquid water at various water saturations and we assume the gas phase is perfectly mobile.

$$k_{rl} = s_l^5 \qquad (2.4)$$
$$k_{rg} = 1 \qquad (2.5)$$

Note that we are not explicitly simulating the dependency of unsaturated properties on swelling in this case. As previously mentioned, the intrinsic permeability for gas flow may be up to six orders of magnitude higher than the intrinsic permeability for liquid flow and the much higher intrinsic permeability is in this case simulated using a high value of the Klinkenberg parameter.

The thermal conductivities of other materials are shown in Table 2.4. In the model, we use all the measured thermal conductivity values from Villar (2012) except those for porous disk and wool. The thermal conductivity of porous disk is not available in Villar (2012). The thermal conductivity of wool is decreased slightly from 0.04 W/mK as reported in Villar (2012) to 0.03 to better match the temperature profile.

Table 2.4. Thermal conductivity of other materials used in the model

Thermal conductivity of porous disk	3.5 W/m-K
Thermal conductivity of Teflon	0.25 W/m-K
Thermal conductivity of foam	0.04 W/m-K
Thermal conductivity of wool	0.03 W/m-K
Thermal conductivity of BT-LV	0.034 W/m-K
Thermal conductivity of air	0.04 W/m-K

2.1.2.3   *Initial and Boundary Conditions*

As described in Villar (2012), the initial condition of the system is as follows: Bentonite pellets have an initial water saturation of 0.22; other materials are completely dry. The system is uniformly at the

atmospheric pressure of 1.01325×10^5 Pa and an ambient temperature of 21.5 ºC. Villar (2012) reported that the relative humidity is 40% before the start of the heating test. The relative humidity is dependent on the water retention curve and temperature, which can be calculated using Kelvin's equation:

$$P_g^W = P_{gS}^W(T)R_H(P_c,T) = P_{gS}^W(T)\exp\left(\frac{-P_c m^W}{\rho_1 RT}\right)$$

(2.6)

$$ln R_H = \frac{-P_c m^W}{\rho_1 RT}$$

(2.7)

The calculated capillary pressure at $R_H = 0.4$ at 21.5 ºC is approximately 1.24×10^8 Pa. The water retention curve used in the model compared with the measured data with bentonite pellets MX-80 (Rizzi et al., 2011) is shown in Figure 2.11.
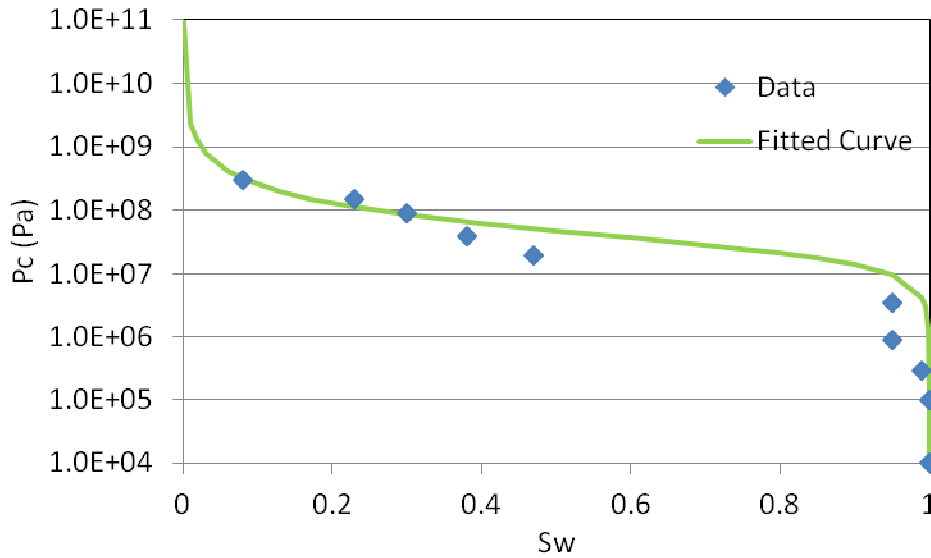
Figure 2.11. Water retention curve in model and measured water retention curve (MX80).

The experiment was conducted in a closed system. No-flow boundary conditions are used for the model. The heater, cooler, and air are simulated by assigning an extremely large specific heat (e.g., 0.5×10^{34} W/kg ºC). The increase of the temperature in the heater is simulated by injecting a large amount of heat to increase the temperature linearly to the target temperatures (e.g., 100 ºC and 140 ºC). The change of the insulation layer is represented in iTOUGH2 by stopping the forward simulation at the time and changing the material type followed by running the simulation using the state condition at the end of the previous run as initial condition.

2.1.2.4   Simulation Results

The simulated results are shown in Figure 2.12. The initial relative humidity was at 40% along the column. With the heater turned on, the simulated relative humidity at 10 cm increases within 200 hours and decreases gradually after that. The simulated relative humidity is lower than the measured relative humidity curve. At 22 cm, the model underestimates the relative humidity but shows similar pattern in relative humidity changes. The relative humidity at 40 cm increases almost linearly. The simulated relative humidity at 40 cm is in excellent agreement with the measured relative permeability. The simulated temperature profile is quite similar to the measured data except the overestimated temperature gradients after 3527 hours. Overall the simulated results are in a reasonable agreement with the measured

data, although we will continue to improve the modeling of this experiment along with the DECOVALEX-2015 project.
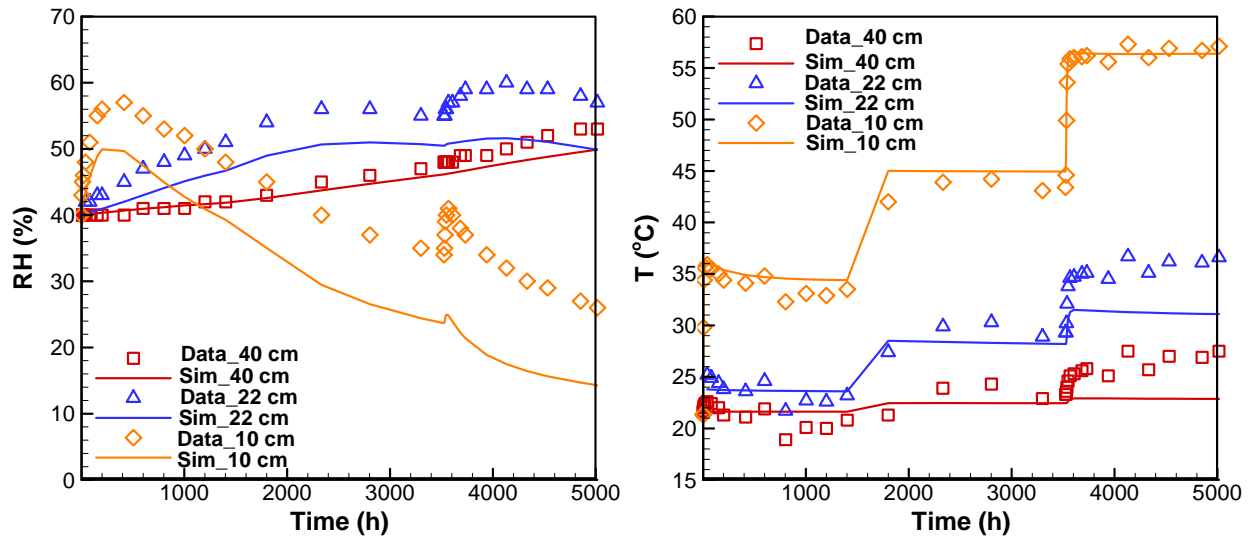
Figure 2.12. Left figure: simulated and measured relative humidity; Right figure: simulated and measured temperature

2.2 Task B2: Horonobe EBS experiment

This task focuses on coupled THMC modeling of a planned full-scale EBS experiment conducted by the Japan Atomic Energy Agency (JAEA) at the Horonobe URL, Hokkaido, Japan (Figure 2.13). The EBS experiment will be carried out at a depth of 350 m in a very porous and soft, siliceous mudstone with the following basic properties

- Porosity 35-60%
- Permeability $10^{-20} – 10^{-18}$ m^2
- UCS (Strength) 5-25 MPa
- Young's Modulus 1-4 GPa
- Thermal Conductivity 1.34-1.53 W/mK

Figure 2.14 show the experimental layout with a vertical heater emplacement installed in a test pit at the bottom of a experimental drift. The experimental drift will be backfilled after the installation of the heater and bentonite buffer into the test pit. The backfill and buffer material will be based on the Japanese Kunigel V1 bentonite. The experimental area will then be isolated by a concrete plug.
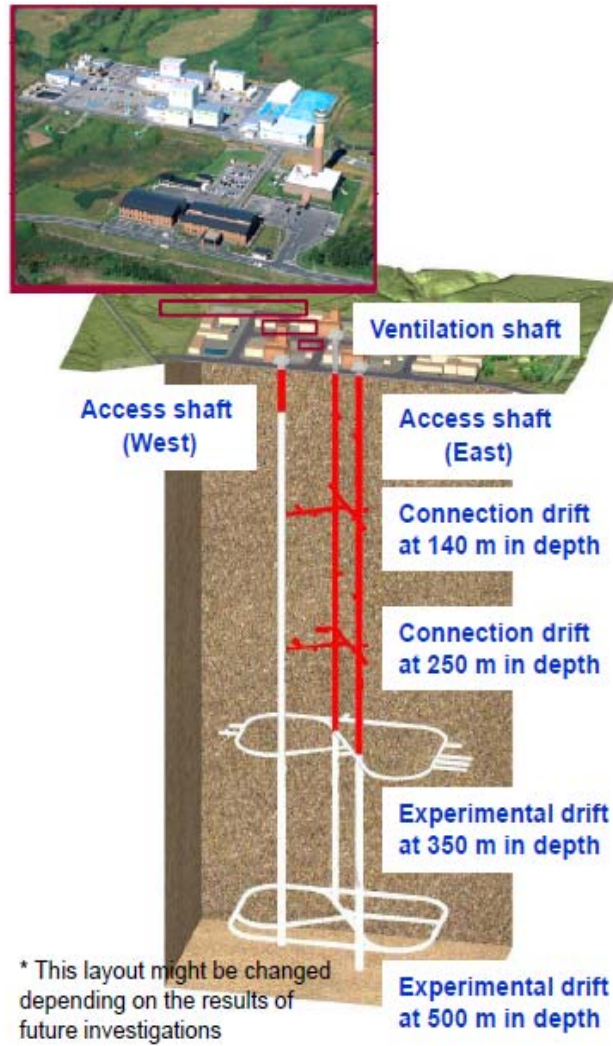
Figure 2.13. Layout of the Horonobe URL in Hokkaido, Japan.
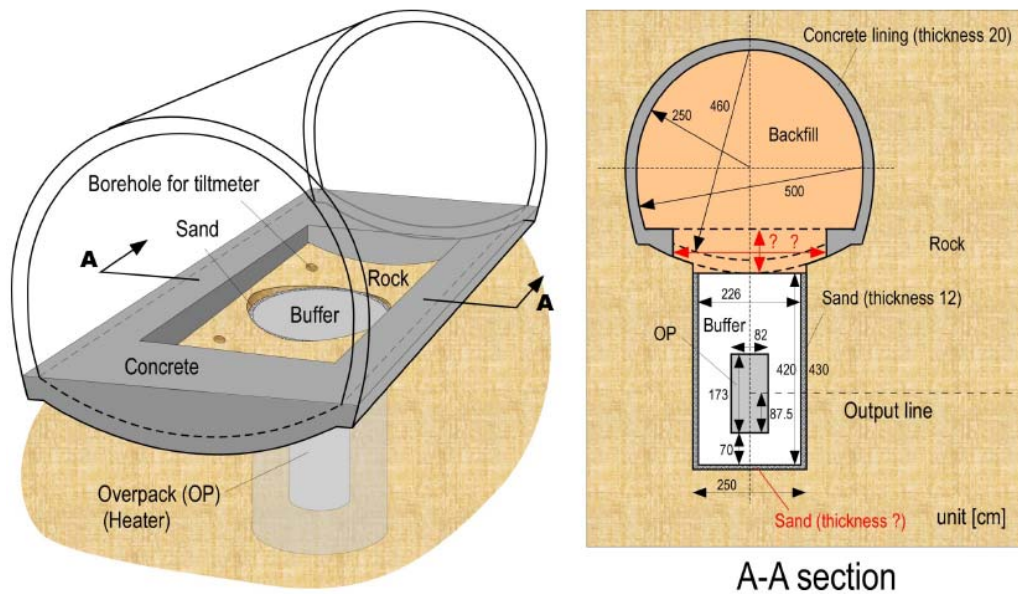
Figure 2.14. General description of the EBS experiment at the Horonobe URL Project in Japan.

Sensors will be installed in buffer, backfill and rock to monitor temperature, stress, strain, pore pressure, humidity, displacement, pH, resistivity, electric potential, and seismic velocity. The detailed layout is not yet fixed and may be changed depending on the initial modeling results.

The DECOVALEX Task B2 is divided into the following steps;

- Step 1 (1D benchmark test)
- Step 2 (prediction analysis 1 and proposal of the sensors layout)
- Step 3 (prediction analysis 2)
- Step 4 (calibration analysis)

The 1D benchmark test will first be performed with exact properties and boundary conditions given by the JAEA. This will be conducted for the teams to familiarize themselves with the problem and for precise comparison of computer codes before going into the more complex full-scale case. Thereafter, a model of the real experimental design will be constructed and a first predictive analysis will be performed for several years from the start of the heating. The results will then be used to guide the installation of sensors that is planned to begin by April 2014. The heating is planned to start in November 2014 and in April 2015 JAEA will provide the monitored data for the first six months of heating to the research teams. The research teams will calibrate their models against this first 6 months of field data and then carry out coupled numerical analysis for long term predictions (100 - 1,000 years) using the test conditions of the EBS experiment. If possible, research teams will also simulate chemical reactions in the buffer material, the rock mass and the groundwater. Output will be the pH and chemical species affected by the concrete lining material.

JAEA will provide reports from the investigations at the Horonobe URL for input parameters related to the mudstone host rock and buffer material properties for the Kunigel V1 bentonite from the previous H12 project, whereas properties for the backfill are still being investigated.

The Task B2 started in May 2013 with Step 1. In the next section we present the preliminary LBNL results for this benchmark.

2.2.1   1D Benchmark Modeling

We first conduct the basic thermal hydrological simulation using the TOUGH2 code. Simulation example results have also been provided by JAEA for an initial comparison. One of the issues in this kind of benchmark is that properties may not be constants, but can for example be functions of temperature and saturation. Also, the properties given by JAEA are based on their modeling approach and their numerical model has been used to calibrate some properties by back-analysis of laboratory experiments. We also conduct simulations using ROCMAS, which uses an approach similar to that of the JAEA simulation model.

2.2.1.1   *Problem set-up*

A thermal-hydrologic model of DECOVALEX task B2 was conducted to make model predictions for temperature, degree of saturation, water content and hydraulic pressure for the system shown in Figure 2.15. The system is a one-dimensional slice of the heater, buffer, and rock from the center of the overpack (which is a heat source) out to 25 m. As shown in Figure 2.15, this includes 0.41 m of the overpack, 0.72 m of the bentonite buffer, and 23.87 m of the rock.
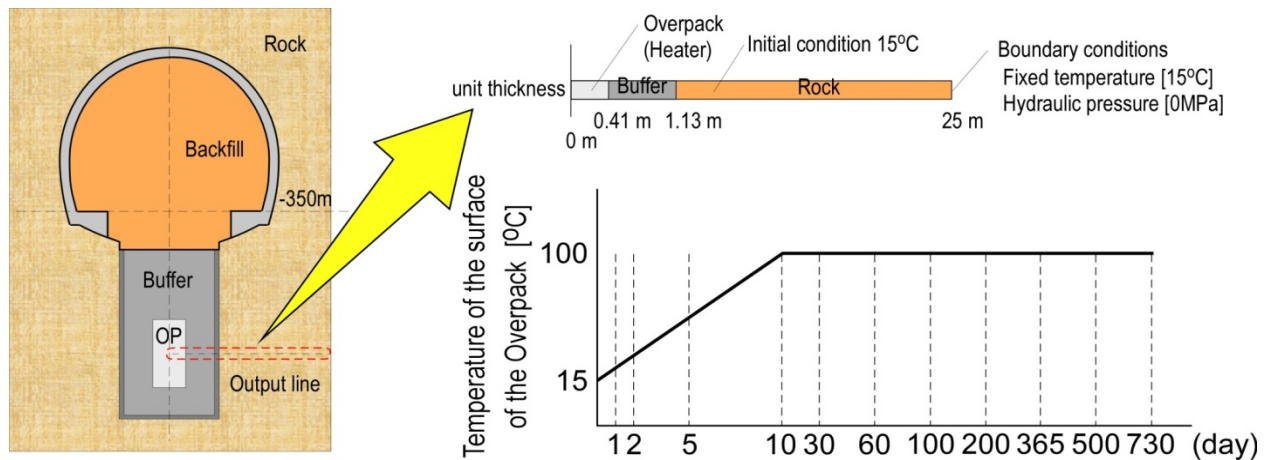
Figure 2.15. DECOVALEX-2015 Task B2 modeling domain and overpack temperature history.

The figure also shows some of the initial and boundary conditions. The initial system temperature is 15° C, and the boundary temperature in the rock is fixed at 15° C. The fixed pressure value at the boundary is 0.10142 MPa pressure, which is one atmosphere pressure and equivalent to a fixed hydraulic gauge pressure of zero. The overpack temperature rises over ten days from 15° C to 100° C and stays there for the duration of the period investigated, 730 days. In addition to the information available from the figure, the rock was also specified to be initially saturated with water and the buffer initially 50% saturated. The rock boundary was also assumed to remain at a fixed saturation of 100%.

2.2.1.2   *Parameterization for TOUGH2 simulation*

For the TOUGH2 simulation, the input parameters of the system are given in Table 2.5.

Table 2.5. Parameters for DECOVALEX Task B2 using TOUGH2

	Overpack	Buffer	Rock
Solids density (kg/m^3)	10,000.	2680.	2454.
Porosity	0.403	0.403	0.4482
Permeability (m^2)	5×10^{-51}	4×10^{-20}	1.33×10^{-15}
Thermal conductivity (saturated) (W/m)	20	1.986	1.231
Specific heat (solids)	10,000	341	626
Thermal conductivity (desaturated) (W/m)	20	0.444	0.579
Klinkenberg parameter (Pa)	8.47×10^{-10}	8.47×10^{-10}	8.47×10^{-10}
Water relative permeability parameter A, (Equation (2.8))	1.3	1.3	NA
Water relative permeability residual saturation, S_r (Equation (2.8))	0	0	NA
Water relative permeability maximum saturation, S_m (Equation (2.8))	1	1	NA
Water relative permeability parameter m, (Equation (2.9))	NA	NA	0.503
Water relative permeability residual saturation, S_r (Equation (2.9))	NA	NA	0
Water relative permeability maximum saturation, S_m (Equation (2.9))	NA	NA	1
Capillary pressure parameter, α (m^{-1}) (Equation (2.10))	8×10^{-3}	8×10^{-3}	9.928×10^{-3}
Capillary pressure parameter, m, (Equation (2.10))	0.375	0.375	0.503
Capillary pressure residual saturation, S_r (Equation (2.10))	0	0	0
Capillary pressure maximum saturation, S_r (Equation (2.10))	1	1	1
Vapor and air diffusion coefficients (m^2/s)	1.44×10^{-5}	1.44×10^{-5}	1.44×10^{-5}

The water relative permeability in the buffer (and overpack) is a power-law relationship given by

$$k_{rw}(S_w) = \left(\frac{S_w - S_r}{S_m - S_r}\right)^A \tag{2.8}$$

The water relative permeability in the rock is given by the van Genuchten relationship:

$$k_{rw}(S_w) = \left(\frac{S_w - S_r}{S_m - S_r}\right)^{1/2}\left[1 - \left\{1 - \left(\frac{S_w - S_r}{S_m - S_r}\right)^{1/m}\right\}^m\right]^2 \tag{2.9}$$

In the buffer (and overpack), the gas relative permeability is the Corey model,

$$k_{rg}(S_w) = \left\{1 - \left(\frac{S_w - S_r}{1 - S_r - S_{gr}}\right)^2\right\}\left\{1 - \left(\frac{S_w - S_r}{1 - S_r - S_{gr}}\right)\right\}^2 \tag{2.10}$$

In the rock, the gas relative permeability is

$$k_{rg}(S_w) = 1 - k_{rw}(S_w) \tag{2.11}$$

Capillary pressure in the buffer (and overpack) and rock are given by the van Genuchten relationship:

$$\psi(S_w) = \frac{1}{\alpha}\left\{\left(\frac{S_w - S_r}{S_m - S_r}\right)^{-1/m} - 1\right\}^{1-m} \tag{2.12}$$

Variations in thermal conductivity and specific heat with water saturation are assumed to be linear between the defined end points. The vapor diffusion coefficient is constant; there is no temperature dependence.

The thermal conductivity and specific heat functions given in the benchmark input were not followed exactly. The following two figures show the comparisons between the benchmark curves and what was used in our model. The maximum specific heat at a water content of about 33% for rock in zone 2 appears to be close to 1500 J/kg-K in the figure provided.
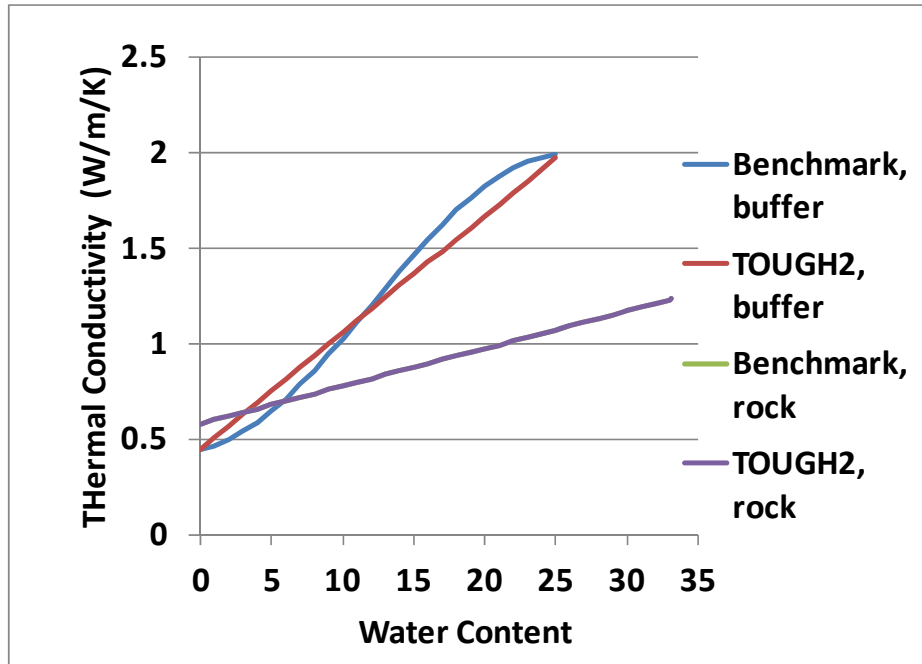
Figure 2.16. Thermal conductivities as functions of water content (the green curve is behind the purple curve).
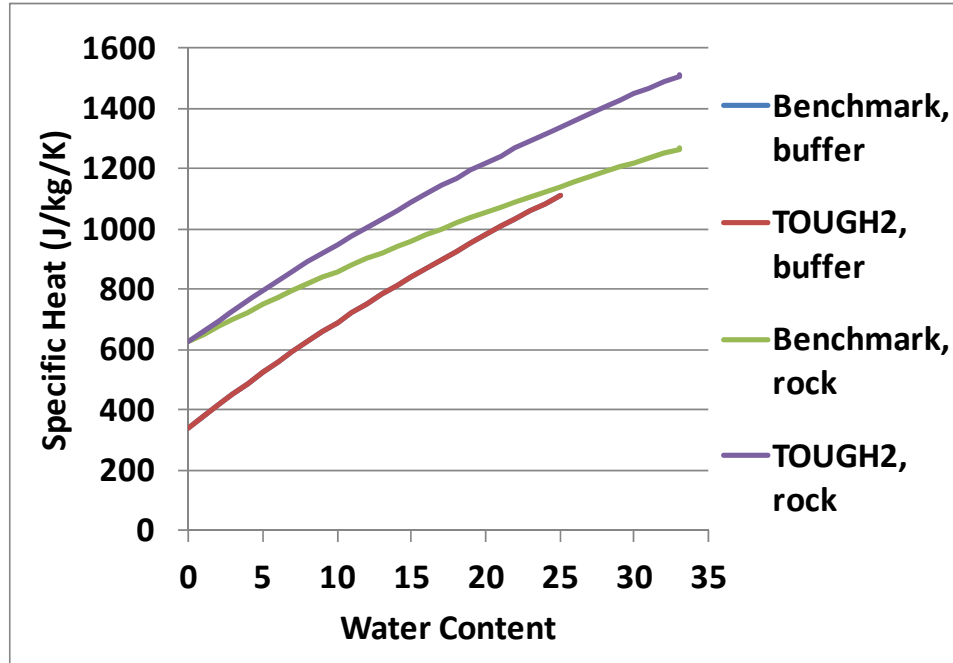
Figure 2.17. Specific heats as functions of water content (the blue curve is behind the red curve).

2.2.1.3   Numerical Model

The problem was solved using the EOS4 equation of state module available in TOUGH2. The following code modifications were implemented:

- In subroutine RELP the gas relative permeability was changed from a constant value of 1 to the relationship given in Equation (2.10) for the relative permeability selection IRP=2. This was done to follow the benchmark input.

- The tortuosity in subroutine MULTI was added as a multiplicative factor to the diffusion coefficient for cases in which the diffusion coefficient is input as a negative number. For this case, $\tau_0\tau_\beta = \tau_0 S_\beta$ instead of $\tau_0\tau_\beta = S_\beta$ in the original code. This was done to use tortuosity for the overpack (set to a small number, 10^{-11}) so that diffusion is suppressed in that material type. Tortuosity for the other material types was set to 1.

- The diffusion driving force in subroutine MULTI was changed from the mass fraction gradient times the phase density to the density gradient of the diffusing component. If the phase density is constant, these two methods give the same result. This was done to avoid instabilities in water saturation.

Table 2.6 gives the cell dimensions along the axis of the 1-D model. The other dimensions of each cell are 1m by 1m. A large-volume cell is also included at the end of the rock section to maintain constant thermodynamic conditions at the rock boundary. The temperature at the overpack was generated by injecting heat into the large-volume overpack cell at a constant rate that raised the temperature from 15 °C to 100 °C over the first 10 days followed by no heat injection over the remaining time period. Because of the large volume of the overpack cell, the temperature remained at 100 °C from 10 to 730 days.

Table 2.6. Numerical discretization

Component	Number of cells	Cell size (m)
Overpack	1	0.41
Buffer	72	0.01
Rock	87	0.01
Rock	50	0.1
Rock	90	0.2

2.2.1.4   Model Results

Model results are given in Figures 2.18, 2.19, and 2.20 for temperature, water saturation, and hydraulic pressure, respectively. The overpack-buffer interface is at x = 0.41 m, the buffer-rock interface is at x = 1.13 m and the far boundary is at 25 m. Time histories are given in Figure 2.21 for water saturation and temperature at the heater (x = 0.41 m) and near the outer edge of the buffer (x= 0.95 m).
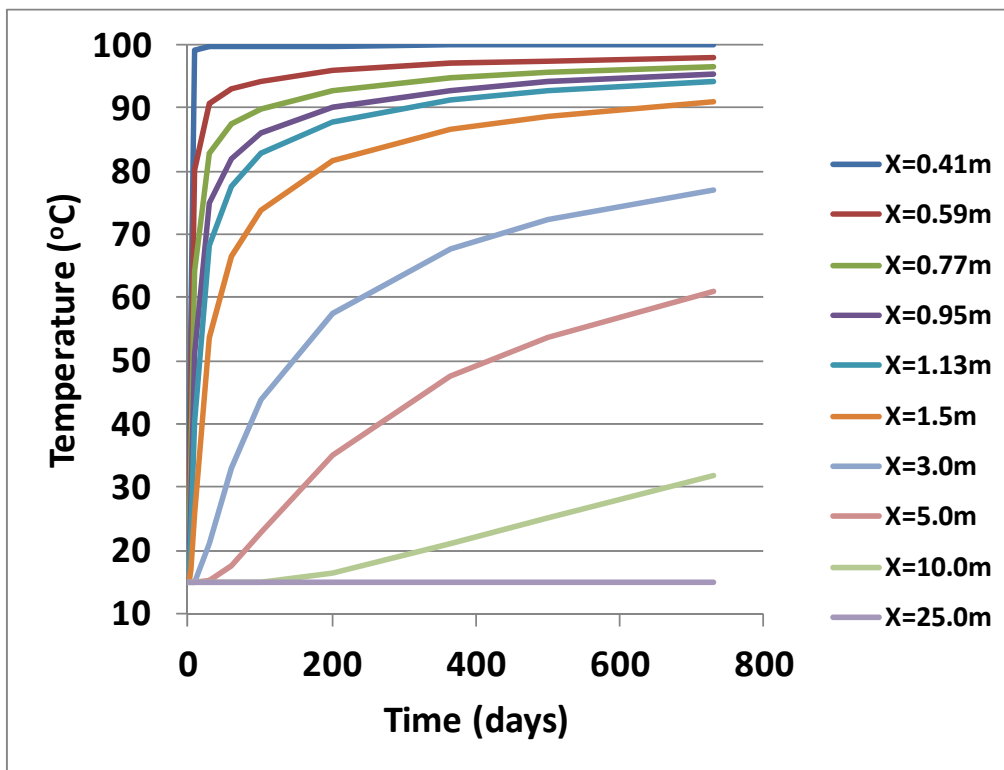
Figure 2.18. Temperature histories at different locations.
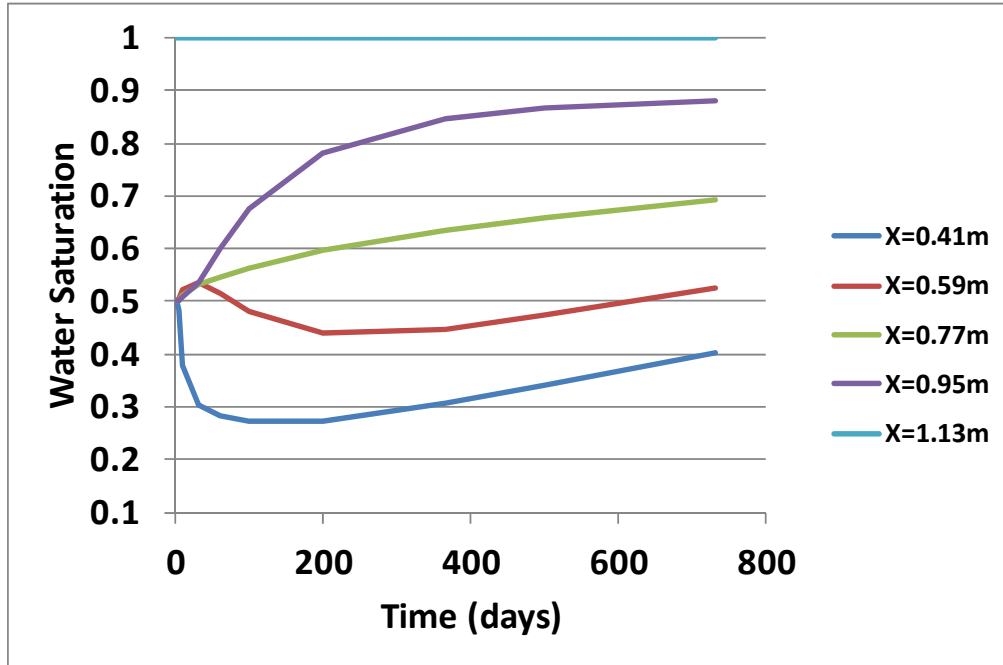
Figure 2.19. Saturation histories at different locations.
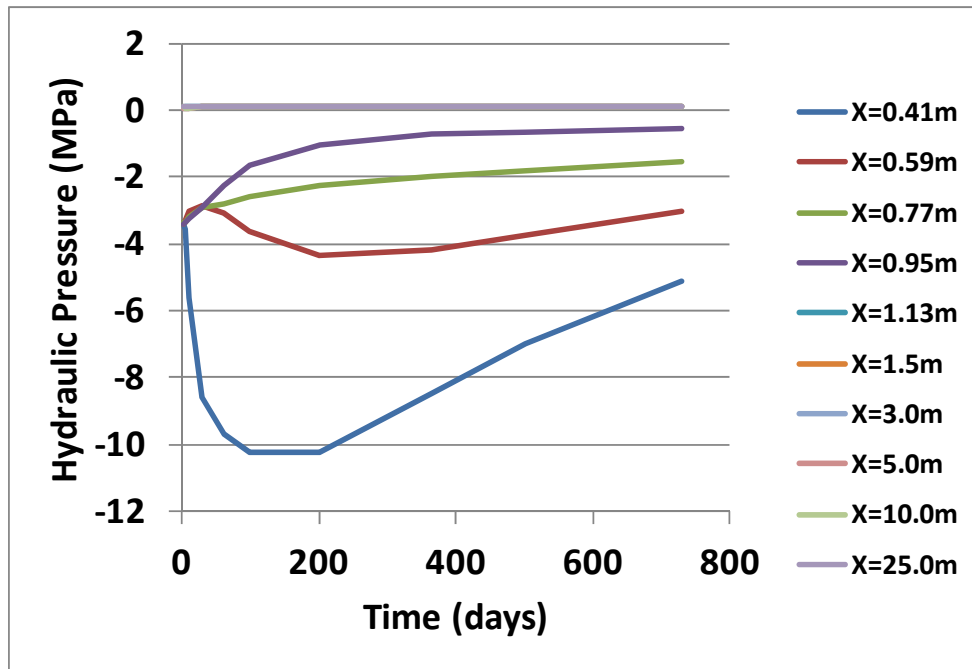
Figure 2.20. Hydraulic pressure histories at different locations.
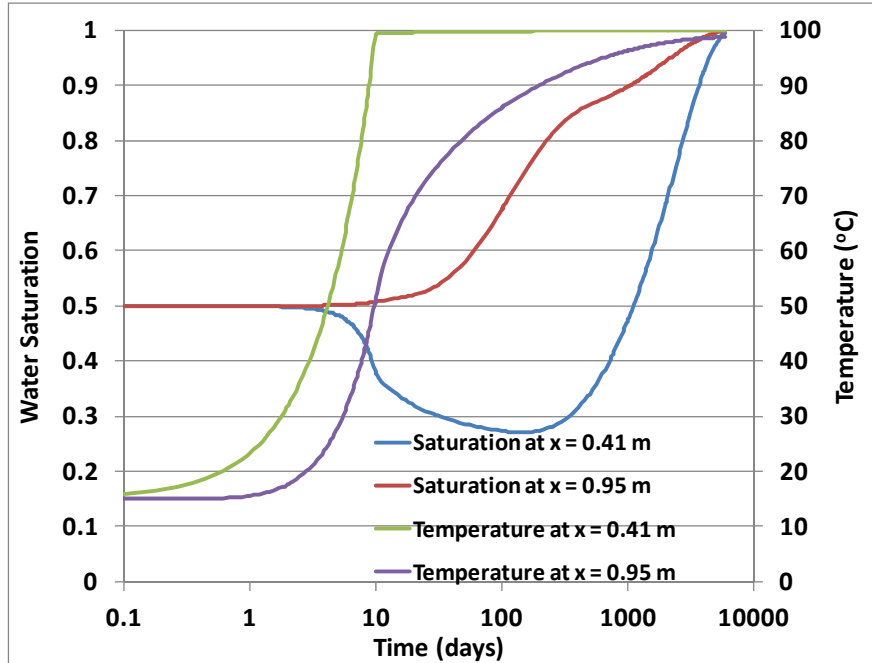
Figure 2.21. Time histories for temperature and saturation at two locations in the buffer.

Another case was also considered. This is where the gas relative permeability is increased by a factor of 10,000 for the buffer. This was implemented by multiplying the gas relative permeability by a factor of 10,000 in subroutine RELP for IRP=2. The results are not significantly different as shown in Figures 2.22 through 2.24, although there is a slight decrease in the minimum water saturation at the x = 0.41 m in Figure 2.23, resulting in a lower hydraulic pressure at that location in Figure 2.24.
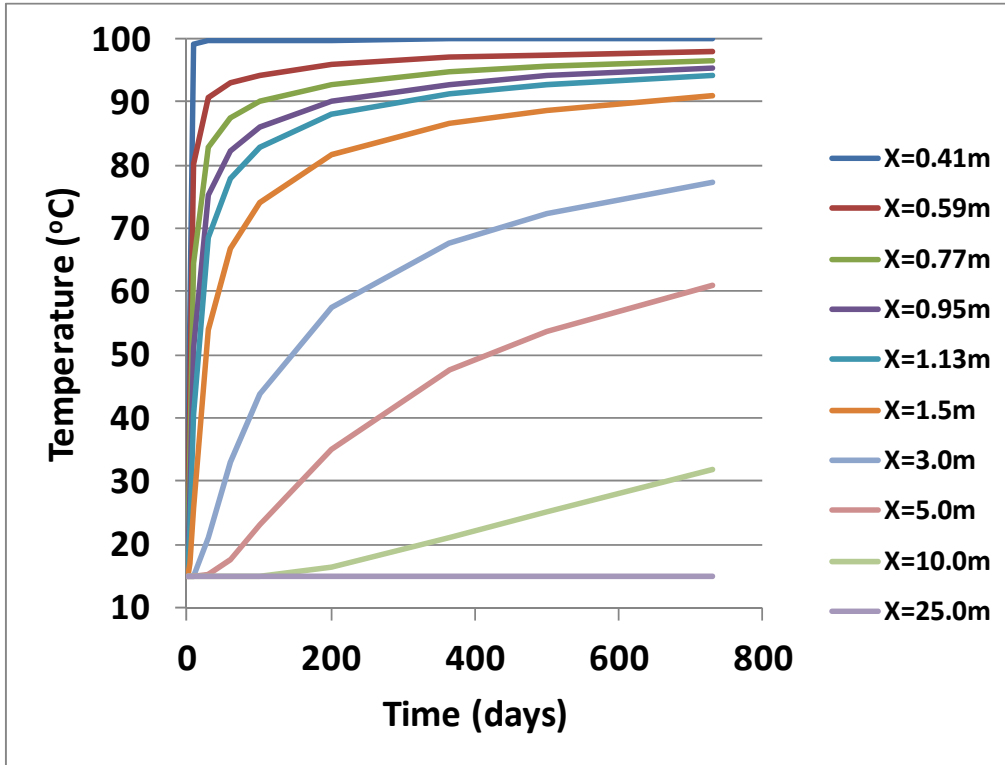
Figure 2.22. Temperature histories at different locations using the high k$_{rg}$.
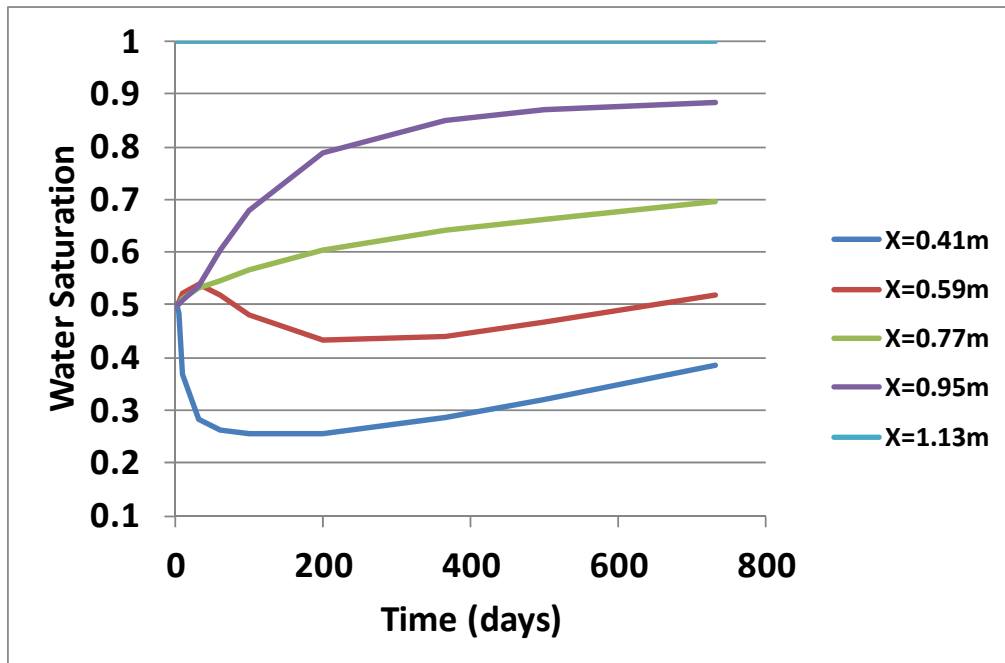
Figure 2.23. Saturation histories at different locations using the high k$_{rg}$.
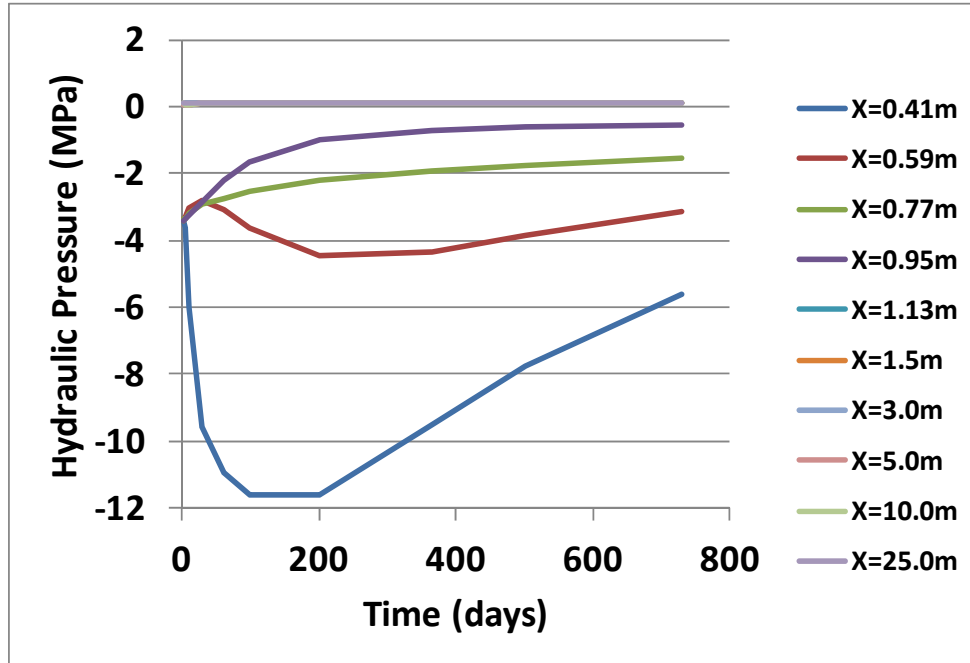
Figure 2.24. Hydraulic pressure histories at different locations using the high k_{rg}.

2.2.1.5   ROCMAS simulation

We conduct an alternative simulation using the ROCMAS code (Rutqvist et al., 2001a) for confidence building and code-to-code comparison. The ROCMAS code has been extensively used for modeling of coupled THM processes in rock-bentonite systems of previous DECOVALEX phases. For example, it was applied to model the Kamaishi Mine heater test in Japan (Rutqvist et al., 2001b). The ROCMAS code models coupled THM processes in partially saturated porous media with single phase liquid flow and vapor diffusion in a static gas phase. It is more similar to the approach used by the JAEA, which is also based on a single phase flow approach. In this approach, the gas phase pressure is assumed to be constant and equal to atmospheric pressure.

In the ROCMAS simulations we assign the exact values of all parameters given in Table 2.5. We do not need to assign parameters related to gas flow because the gas phase is assumed to be a passive spectator at constant pressure.

The simulation results shown in Figures 2.25 through 2.28 are very similar to corresponding TOUGH2 simulation results in Figures 2.18, through 2.21. The temperature evolution is practically identical, whereas some slight differences can be observed in the evolution of saturation and pressure. Such slight differences in saturation are not surprising considering the different approaches (full two-phase flow versus single phase flow) that are used. Considering the very good agreement it appears that the single phase approach used in ROCMAS is sufficient in this case.
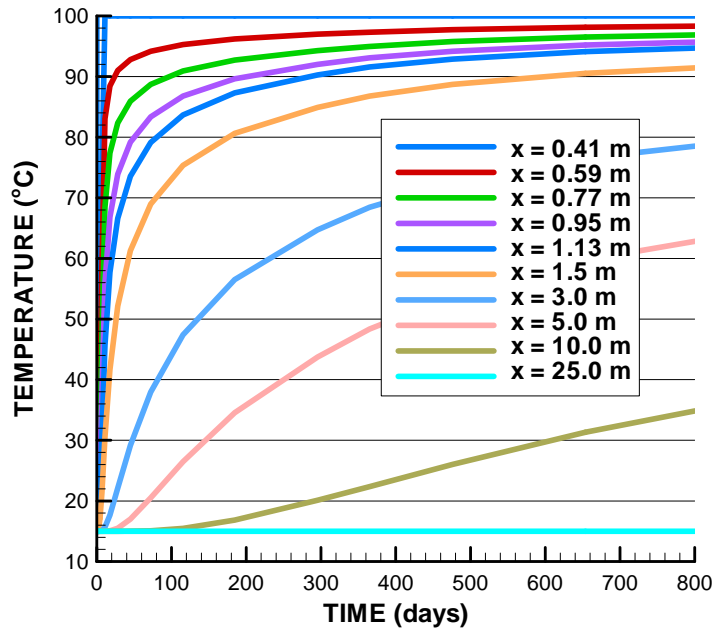
Figure 2.25. Temperature histories at different locations for ROCMAS simulation.
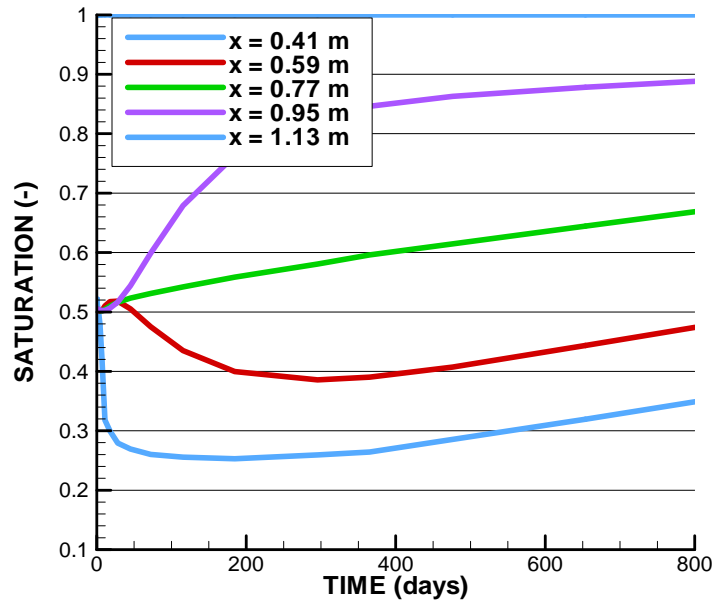
Figure 2.26. Saturation histories at different locations for ROCMAS simulation.
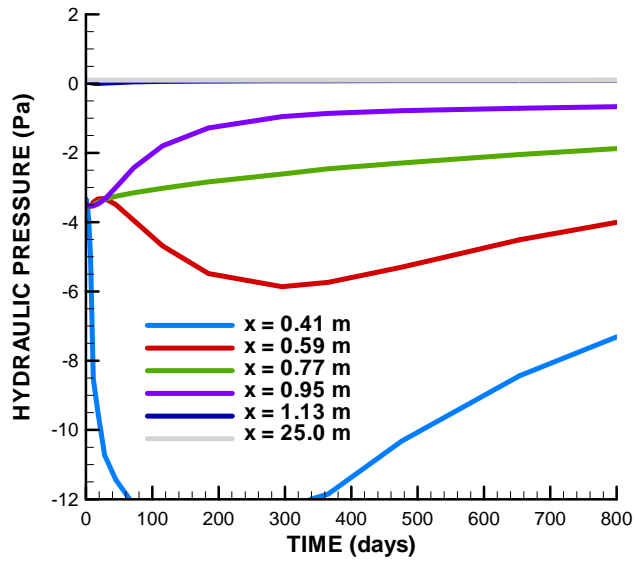
Figure 2.27. Hydraulic pressure histories at different locations for ROCMAS simulation.
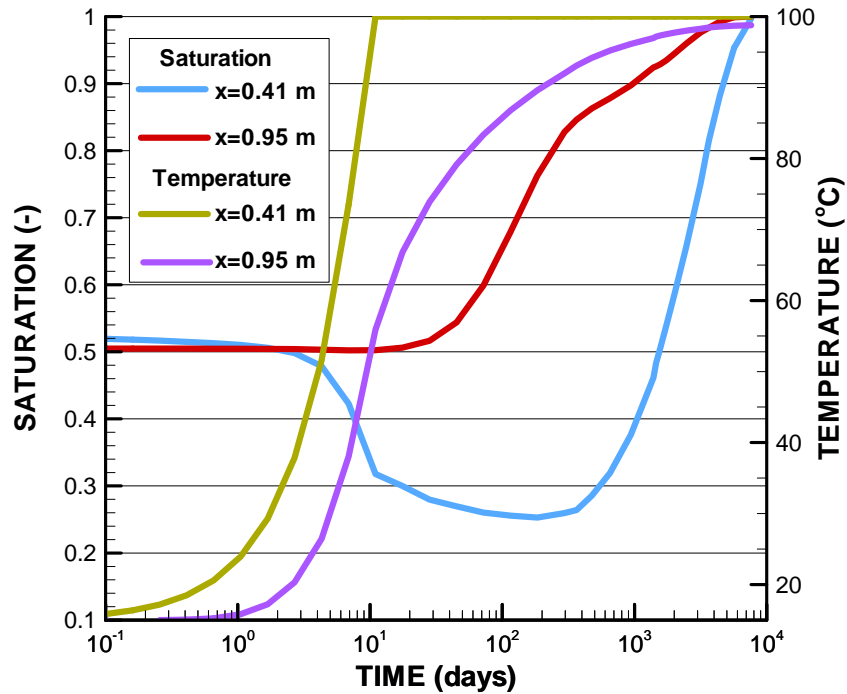
Figure 2.28. Time histories for temperature and saturation at two locations in the buffer for ROCMAS simulation.

2.3   THM MODELING STATUS AND PLANS

We are now one year into the participation of the DECOVALEX-2015 project. At the same time, we have conducted significant model developments related to the THM modeling of bentonite and clay rock. In this situation it is extremely valuable to have access to field and laboratory data for testing and validation of the newly developed models. In addition to the modeling of field experiments we are currently conducting a number of benchmark tests which enable us to compare our models to other models that are part of the DECOVALEX-2015 project. The modeling of the HE-D in situ heater test at Mont Terri has been completed showing good agreement with field data and other models in the DECOVALEX-2015 project. We are currently focusing on parameterization of bentonite properties through modeling of laboratory experiments and benchmarks; both related to the modeling of the Mont Terri URL HE-E heater test and the Horonobe URL EBS experiment. This work will be presented at the next DECOVALEX-2015 workshop at Mont Terri in November 2013. Thereafter, new model predictions will be performed related to both the Mont Terri URL HE-E experiment and the Horonobe URL EBS experiment.

3.   MODELING REACTIVE DIFFUSIVE TRANSPORT

Clay-rich rock, like engineered clay barriers, have remarkable macro-scale properties such as high swelling pressure (Gonçalvès et al., 2007), very low permeability (Mammar et al., 2001), semi-permeable membrane properties (Malusis et al., 2003), and a strong coupling between geochemical, mechanical, and osmotic properties (Malusis and Shackelford, 2004; Gonçalvès et al., 2007). These properties are thought to arise from the distinct geochemical, transport, and mechanical properties of the interlayer nanopores of swelling clay minerals such as Na-montmorillonite and other smectites (Gonçalvès et al., 2007), as well as the non-swelling clays like illite. An important feature of the clays is the high negative charges typically present on the mineral surfaces, which results in a substantial Electrical Double Layer (EDL) that may make up a significant fraction of the porosity in the rock. This is certainly one of the reasons why clay-rich rocks like the Opalinus Clay in Switzerland are being considered as host rocks for geological nuclear waste repositories. The isolation potential of Opalinus Clay is determined by its physical and chemical properties. Hence, the main interest is in its permeability and capacity for self-sealing, as well as the diffusion behavior of radionuclides. The diffusion behavior of radionuclides and their retention potential are being investigated in the DR-A (diffusion and retention) experiment, for example. In a small borehole, an isolated test interval is saturated with water and a controlled amount of tracer material (e.g. tritium) is then introduced. After at least a year, the small borehole is overcored. In the new, larger core, investigations are then carried out to determine how far the tracer has penetrated into the rock. In the process, non-sorbing radionuclides (e.g. tritium) migrate more quickly than strongly sorbing radionuclides (e.g. cesium) that will be present in a high-level waste repository. In addition, as in engineered clay barriers, anion exclusion is an important effect that slows the rate of diffusion of the anions. The rate of diffusion is also monitored by tracking the chemistry of a borehole that is injected with a cocktail at a specified time.   The rate of decrease of the constituents of the cocktail give an indication of the rate of diffusion of the anions, cations, and uncharged species through the Opalinus Clay, making it possible to assess the feasibility of using it as a natural barrier system for a geological nuclear waste repository.

This section describes a modeling approach for simulating the out-diffusion of tracers and ions from the DR-A borehole test in Opalinus Clay at Mont Terri site. Use is made of a new model for diffusive transport that includes an explicit Electrical Double Layer (EDL) model (CrunchEDL), which is described in detail below.

3.1   Mathematical and Numerical Formulation

Since the clays in rock like the Opalinus Clay typically possess a strong negative surface charge, the Electrical Double Layer (EDL) bordering the clays are enriched in cations and depleted in anions. The anions are said to be "excluded", although only in the very smallest nanopores (typically less than 1 micron) are anions excluded altogether.   Since the EDL porosity can constitute a significant fraction of the total porosity, it is important to have a mechanistic model to describe its behavior, especially the diffusive transport of ions within it. A rigorous model for the electrical double layer (EDL) can be derived from the combination of several equations, including the Poisson equation describing the distribution of electrical potential, ψ, in water

$$\nabla^2 \psi = -\frac{\rho_z}{\varepsilon}, \tag{3.1}$$

where ε is the permittivity and ρ_z is the volumetric charge density given by

$$\rho_z = e \sum_i z_i C_i.$$
(3.2)

In Equation 3.2, e is the elementary charge of the electron, z_i is the valence of the ion, and C_i is the concentration bulk solution. The Boltzmann distribution gives an expression for the concentration, $C_i^{EDL}(z)$, in the electrical double layer as a function of distance from the charge solid surface, z,

$$C_i^{EDL}(z) = C_i \exp\left(\frac{-z_i e \psi(z)}{k_B T} \right),$$
(3.3)

where k_B is the Boltzmann constant, and T is the absolute temperature. Combining Equation 3.3 with the Poisson equation (Equation 3.1) yields the Poisson-Boltzmann equation (Schoch et al., 2008)

$$\nabla^2 \psi = \frac{-e}{\varepsilon} \sum_i z_i C_i \exp\left(\frac{-z_i e \psi(z)}{k_B T} \right)$$
(3.4)

which can be solved exactly for various simple formulations (e.g., the Gouy-Chapman model, which assumes a symmetric electrolyte).

Integrating the Poisson-Boltzmann equation over nanometer length scales from charged mineral surfaces, however, was not practical in the present version of CrunchEDL (a reactive transport simulator developed by Carl Steefel) because of the desire to consider larger length scales, so an alternative approach based on a Donnan Equilibrium model (Wersin et al., 2004; Leroy and Revil, 2004; Appelo et al., 2007; Leroy et al., 2007; Appelo et al., 2008; Birgersson and Karnland, 2009; Tournassat and Appelo, 2011) is used. The electrical double layer is conceptualized as consisting of two parallel layers of charge, one being the surface charge associated with direct sorption at the mineral surface (the Stern layer, typically divided into an inner and outer Helmholtz layer), and the second being the diffuse layer charge, a swarm of counterbalancing ions (Figure 3.1).
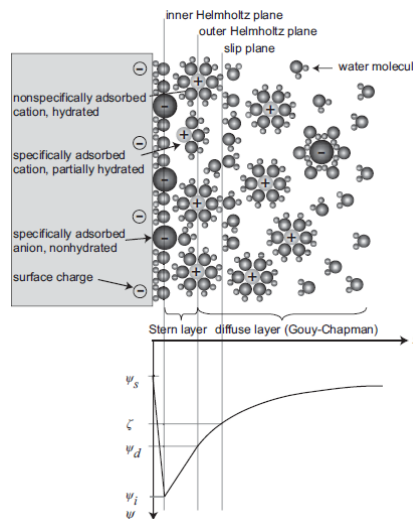
Figure 3.1. Schematic illustration of the Gouy-Chapman-Stern model of the solid-electrolyte interface, with the potential distribution $\psi(z)$ versus distance from the charged solid surface. The diffuse layer is defined beyond the outer Helmholtz plane (from Schoch et al., 2008).

In the approach taken in CrunchEDL, the chemical potentials of the species in the diffuse layer and the bulk solution are equated. Writing equations for the chemical potentials of the species i in the bulk solution (or macroporosity) (superscript "B") and electrical double layer (superscript "EDL") respectively, we have

$$\mu_i^B = \mu_i^{B,0} + k_B T \ln a_i^B$$
$$\mu_i^{EDL} = \mu_i^{EDL,0} + k_B T \ln a_i^{EDL} + q_i \psi_m$$

(3.5)

where the superscript 0 (first term on the right-hand side) refers to the chemical potential at the reference state, a_i are the species activities, q_i, is the charge of an ion (the elementary charge of a particle, e, multiplied by the valence of the ion, z_i), and ψ_m is the mean electrical potential in the electrical double layer. The condition of Donnan Equilibrium implies that

$$\mu_i^{EDL} = \mu_i^B$$
$$\mu_i^{EDL,0} = \mu_i^{B,0}$$

(3.6)

Combining Equations 3.3, 3.5, and 3.6 and assuming that the activity coefficients for the diffuse layer and bulk solution are the same gives the Boltzmann distribution for the ion activities in the electrical double layer, C_i^{EDL}:

$$C_i^{EDL} = C_i^B \exp\left(\frac{-z_i e \psi_m}{k_B T}\right).$$

(3.7)

The diffuse layer charge balances the charge within the Stern layer, Q^{SL}, which may consist in CrunchEDL of either a fixed mineral charge due to vacancies in the mineral structure (as in the case of classical ion exchange), or of fixed mineral charge modified by inner sphere and out sphere complexes developed within the Stern layer calculated with a surface complexation model:

$$\phi^{EDL} \sum_i z_i C_i^{EDL} = Q^{SL}$$

(3.8)

where ϕ^{EDL} is the volume (or porosity) of the electrical double layer. The left-hand side of Equation 3.8 gives a volumetric charge density in units of charge equivalents per unit volume porous medium. The surface charge is given by

$$Q^{SL} = \sum_k^{Ns} z_k \Gamma_k$$

(3.9)

where Γ_k is the concentration in units of moles sorbed species per unit volume porous medium and z_k is the valence of the surface complex. In the CrunchEDL approach, therefore, one new equation is introduced (Equation 3.8), with one new unknown, the mean electrostatic potential of the diffuse layer, ψ_m. Note that in this formulation, the concentrations of the ions in the diffuse layer are dependent (or secondary) species that are calculated algebraically from the knowledge of the bulk solution composition and the mean electrostatic potential. A kinetic treatment of the diffuse layer ions would require that they be considered as primary unknowns.

Several approaches are available for calculating the fixed or Stern layer charge that is balanced by an electrical double layer. Even if the full Poisson-Boltzmann (PB) equation is used, special consideration

needs to be given to the charge present in the Stern layer, a feature not always seen in the simpler implementations of the Poisson-Boltzmann equation. The starting point is the fixed mineral charge, which is normally given by the cation exchange capacity. If no Stern layer sorption occurred, the fixed mineral charge would provide a Dirichlet boundary condition for the electrostatic potential, ψ_f, at the solid surface,

$$\psi(0) = \psi_f \tag{3.10}$$

In the case of no Stern layer sorption, therefore, the PB equation can be integrated across the entire thickness z of the electrical double layer. In the case where the charged bentonite particles are bordered by bulk water, this would be the point in space where the local solution becomes electroneutral (where the electrostatic potential goes to zero). In the case of overlapping double layers, as considered by Gonçalvès et al. (2007) and Schoch et al. (2008), this would be the midpoint between the two charged clay (or solid) surfaces.

3.1.1 Dynamic Calculation of Electrical Double Layer Thickness

CrunchEDL also now includes a dynamic calculation of the electrical double layer porosity, ϕ^{EDL}, based on the diffuse layer thickness as a function of ionic strength according to

$$\phi^{EDL} = A_{clay}\lambda_{DL}D_L = A_{clay}\lambda_{DL}\frac{\beta_{DL}}{\sqrt{I}} \tag{3.11}$$

where D_L is the Debye length, λ_{DL} gives the multiples of the Debye length used in calculating the electrical double layer porosity (as in the approach of Tournassat and Appelo, 2011), β_{DL} is a temperature-dependent factor (= 2.15×10^{-10} meters at 25°C), I is the ionic strength of the bulk solution, and A_{clay} is the surface area of the charged mineral surfaces (normally clays). The Debye length provides an approximate measure of the width of the electrical double layer, although in their Donnan or mean electrostatic model, Tournassat and Appelo (2011) included as many as five Debye lengths to describe the EDL porosity.

Previously we have presented results in which the ionic strength is constant over the domain. It is also possible, however, to consider transient cases in which a salinity front propagates through the domain, changing the Debye length and thus the diffuse layer porosity dynamically. Note that in this case, the EDL thickness and thus the transport properties of the compacted bentonite are modified by the changing ionic strength. The effect is different from the swelling behaviour described in Section 2, and may in fact work in the opposite way.

In the CrunchEDL approach, in which solute mass is tracked in both the bulk porosity and the diffuse layer (EDL) porosity, this gives an accumulation term (neglecting liquid saturation) of

$$\frac{\partial\left[\phi^B C_i^B + \phi^{EDL}C_i^{EDL}\right]}{\partial t} = \frac{\partial\left[\phi^B C_i^B + \left(A_{clay}\lambda_{DL}\beta_{DL}\Big/\sqrt{I}\right)C_i^{EDL}\right]}{\partial t}. \tag{3.12}$$

In this case, the bulk porosity is treated as a constant, or at least as separately determined or fixed. Since the total porosity then can increase or decrease as the EDL thickness changes, special considerations need to be made to conserve mass in the system. Alternatively, it is preferred to treat the total porosity (bulk and EDL) as constant, in which case the bulk and EDL porosities would be updated according to:

$$\frac{\partial\left[\left(\phi^{Tot}-\phi^{EDL}\right)C_i^B+\phi^{EDL}C_i^{EDL}\right]}{\partial t}$$

(3.13)

where ϕ^{Tot} is the total porosity = $\phi^B+\phi^{EDL}$.

3.2   Application to the DR-A Diffusion Test at Mont Terri, Switzerland

To test the EDL transport model developed and described here, we have used it to simulate non-reactive and reactive transport processes in the DR-A experiment at Mont Terri in Switzerland. The Mont Terri site consists of Opalinus Clay, a primarily marly claystone with differing proportions of sand and carbonates, and is about 180 million years old. The stratigraphic section in which the Mont Terri site is located is shown in Figure 3.2. The Opalinus Clay is characterized by a very low permeability, which makes diffusion the dominant mode of solute transport (in this respect, similar to compacted bentonite under normal conditions).
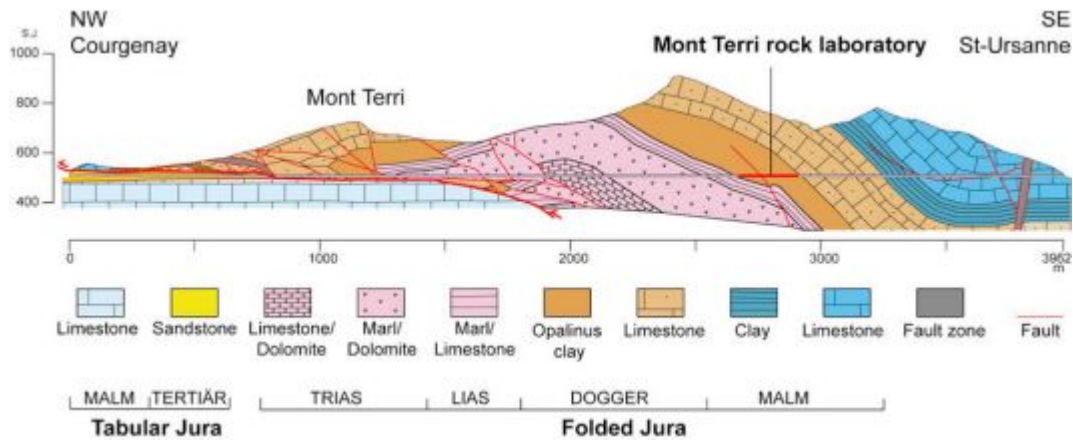
Figure 3.2. Stratigraphic section of the Jura Mountains in which the Mont Terri rock laboratory is located.

The DR-A test has consisted of a single borehole drilled in the Opalinus Clay that contains a constant ionic strength cocktail and anions, cations, and non-reactive tracers like tritium (HTO). Figure 3.3 shows the location of the DR-A niche in map view. Figure 3.4 shows the experimental setup used for the earlier DI-A test at Mont Terri, similar in setup to what has been used for the DR-A test. A volume of cocktail in excess of the actual cylindrical volume of the borehole is used as reservoir. This is treated in CrunchEDL by defining a capacity factor, α (= 2.175), that represents the additional volume needed to accommodate the extra solution volume (11.2 L) available to the actual borehole volume. In the first stage through Day 189, the borehole cocktail is a 0.384 M ionic strength solution dominated by sodium (Table 3.2). At Day 189, a higher ionic strength solution (1.135M) was circulated in the borehole apparently without diluting the tracers (HTO, iodine, and bromine) in the cocktail. The higher ionic strength was made up of both Na^+ (0.50M) and K^+ (0.56M) and Cl^- (1.13M) and was allowed to diffuse out of the borehole through Day 412.

3.2.1   CrunchEDL Simulation of DR-A Test

3.2.1.1   *DR-A Simulation Parameters*

In the simulations, a total porosity of 0.15 was assumed for the Opalinus Clay. The total porosity was treated as fixed, with partitioning between the "bulk" and "EDL" porosities governed by the Debye length (determined by the ionic strength, and thus variable over the course of the 412 day experiment). For Case 1 (Figure 3.5), four Debye lengths were used to calculate the EDL porosity according to Equation 3.11. For Case 2 (Figure 3.6), six Debye lengths were assumed. The dynamic Debye length and result partitioning between bulk and EDL porosity was calculated using Equation 3.12. The additional volume needed to accommodate the extra solution volume (11.2 L) available to the actual borehole volume (Table 3.1) was treated in CrunchEDL by defining a capacity factor, α (= 2.175).

Table 3.1. Physical parameters for DR-A test

Length of injection interval	104 cm
Length of filter screen	67 cm
Volume of circulation system	11.2 L
Borehole diameter	76 mm
Filter, outer diameter	70 mm
Filter, inner diameter	62 mm
Filter, porosity	45%
Gap between filter and borehole wall	3 mm
Central tube, outer diameter	61 mm
Dip of bedding	32.5º
Porosity of Opalinus Clay	15%

Figure 3.3. Plan view of the Mont Terri site showing location of DR-A niche.

Figure 3.4. Schematic of the experimental setup from the DI-A test, similar in concept to the DR-A test.

Table 3.2. Geochemistry of borehole solution, with higher ionic strength used 189-413 days.

Species (Total)	0-189 Days	189-413 Days
	(M)	(M)
Ionic Strength	0.384	1.135
pH	4.16	7.60
Ca^{2+}	0.0188	0.0230
Mg^{2+}	0.0180	0.0147
Na^+	0.259	0.500
K^+	0.0016	0.560
Cl^-	0.300	1.113
SO_4^{2-}	0.0137	0.00024
HCO_3^-	0.00328	0.00050
Sr^{2+}	0.00051	0.00045
Cs^+	0.00027	0.0000062
I^-	0.0109	0.0109
Br^-	0.0109	0.0109
HTO	1.000	1.000

For the simulation, a preliminary estimate of the illite specific surface area (200 m2/g) and volume fraction (0.25) was made for the Opalinus Clay, which is the material expected to provide most of the retardation. A fixed mineral charge of 200 μequivalents/g illite was assumed, all of which is compensated by the electrical double layer (i.e., no Stern Layer sorption was allowed). Cylindrical coordinates were

used in the simulations, with the assumption that the system was axisymmetric—thus, the system is modeled in a 1D plane.
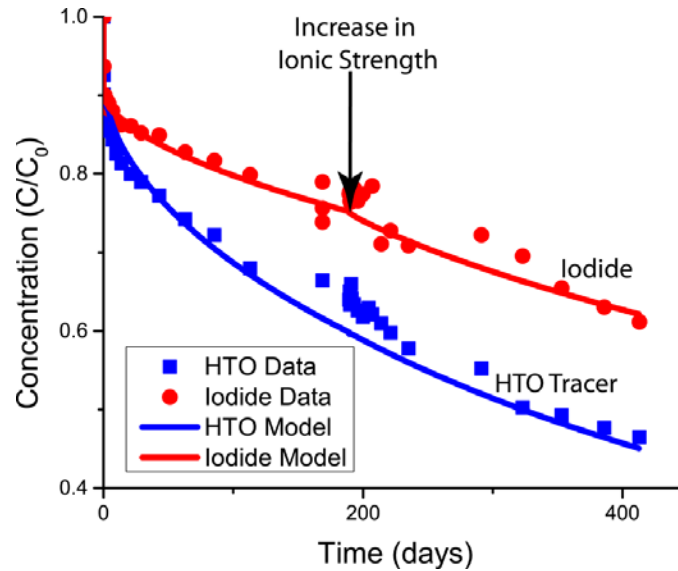

3.2.1.2   *DR-A Simulation Results*

In both cases, a high value for the diffusion coefficient of solutes in the filter has been used to avoid a limitation on the rate of loss from the borehole due to this material. In Case 1 (Figure 3.5), a diffusion coefficient of $2.7x10^{-10}$ m^2/s was assumed for all of the species in the Opalinus Clay, with the exception of the anions, for which a value of $1.25x10^{-10}$ m^2/s was used. As an initial test, the same values for the diffusion coefficients were used in the bulk and EDL porosity, although this assumption abandoned in Case 2 (Figure 3.6) so as to optimize the fit to the ionic strength effect.

Results for Case 1, with the increase in ionic strength in the borehole-reservoir system at Day 189, are shown in Figure 3.5. It should be noted that the anion (iodide and bromide) breakthrough data shows a slight increase in the rate of loss from the borehole starting about Day 189, the time when the ionic strength was increased. There is a mismatch with the HTO data, but close inspection shows that it follows the same exponential decay curve (i.e., the slope of the concentration versus time profile continuously decreases).   Figure 3.6 shows that the HTO can be modeled as a single decaying curve. The simulation results in Figure 3.5 show only a very small increase in the rate of loss from the borehole (solid line red for iodide), apparently the result of the use of the same diffusion coefficients for the iodide and bromide in the EDL and bulk porosity. One expects that diffusion rates of anions in the EDL are smaller because of the greater tortuosity for the negatively ions versus the bulk fluid. Note that the data shows a stronger effect of the ionic strength, with the rate of loss from the hole increasing more dramatically for the anions at about Day 290. This effect is in keeping with a decrease in the thickness of the EDL, and thus an increase in bulk versus EDL porosity that follows from Equation 3.11. This is in contrast to some of the predictions based on swelling behavior alone that would have the effect of an increase in ionic strength reducing the bulk porosity. If the only effect of an increase in ionic strength was on the swelling behavior of the clays, then one would expect a less (not more) rapid loss of anions from the borehole.
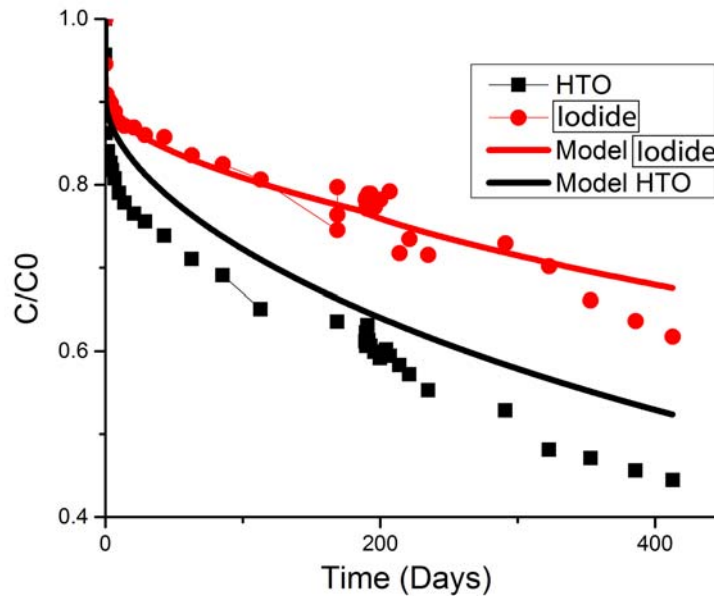
Figure 3.5. Data (symbols) versus simulation results (solid lines) for the DR-A test through Day 412 for Case 1 in which diffusion coefficients are the same in the bulk and EDL porosity and 4 Debye lengths make up the EDL porosity.

As a contrast, compare a simulation in which all species (anions, cations, and uncharged species) are characterized by diffusion coefficients of 4×10^{-10} m^2/s in the bulk porosity, while in the EDL porosity the cations and uncharged species have diffusion coefficients of 1×10^{-10} m^2/s and the anions have diffusion coefficients of 5×10^{-11} m^2/s (i.e., nearly an order of magnitude lower than in the bulk porosity). In order to get an improved fit with the data, it is also necessary to increase the number of Debye lengths considered as making up the EDL porosity to 6 from the value of 4 used in the simulations shown in Figure 3.5. When a value of 6 Debye lengths is used, then the EDL porosity makes up approximately 50% of the total porosity of the Opalinus Clay. As shown in Figure 3.6, with this model the increase in ionic strength results in an increase in the rate of out-diffusion in the simulation results (see change in slope at 189 days).

Figure 3.6. Data (symbols) versus simulation results (solid lines) for the DR-A test through Day 412 for Case 2 in which diffusion coefficients for anions are nearly one order of magnitude less in the EDL porosity than in the bulk porosity. 6 Debye lengths are considered for the EDL porosity in this case.

Table 3.3. Opalinus Clay Properties and Simulation Results

	Case 1 (Figure 3.5)		Case 2 (Figure 3.6)	
	0-189 Days	189-413 Days	0-189 Days	189-413 Days
Illite Specific Surface Area	200 m^2/g	200 m^2/g	200 m^2/g	200 m^2/g
Illite Volume Fraction	0.25	0.25	0.25	0.25
Fixed Charge of Illite	200 μeq/g	200 μeq/g	200 μeq/g	200 μeq/g
EDL Porosity (equilibrated w/ borehole)	0.076	0.049	0.113	0.074
Number of Debye lengths	4	4	6	6
Na$^+$ Concentration in EDL (equilibrated)	0.253	0.661	0.380	0.586
K$^+$ Concentration in EDL (equilibrated)	0.0029	0.335	0.0025	0.320
I$^-$ Concentration in EDL (equilibrated)	0.0046	0.0049	0.0054	0.0051

4.   CONCLUDING REMARKS

LBNL's international activities related to THM and reactive transport model development currently include modeling of field experiments at the Mont Terri URL, Switzerland, and Horonobe URL, Japan. It is DOE's participation in international projects such as DECOVALEX and Mont Terri that enable us to test our new model developments against relevant field and laboratory data.

Relate to THM modeling of EBS components, we are currently focusing on parameterization of bentonite properties through modeling of laboratory experiments and benchmarks; both related to the modeling of the Mont Terri URL HE-E heater test and the Horonobe URL EBS experiment. This work will be presented at the next DECOVALEX-2015 workshop at Mont Terri in November 2013. Thereafter, new model predictions will be performed related to both the Mont Terri URL HE-E experiment and the Horonobe URL EBS experiment.

Related to reactive diffusive transport modeling, we have carried out preliminary simulations of the DR-A test, including the increase in ionic strength at Day 189. The anion exclusion effect seems to lessen (the rate of out-diffusion thus increases) when the ionic strength is increased, although this is not currently fully captured by the simulations. It appears that lower diffusion coefficients in the EDL for the anions are required to capture this effect. The objective of the FY14 work will be to refine the EDL-explicit model to the current DR-A experiment, out through 412 days. The major focus will be to establish the effect of the increase in ionic strength and its effect on anion exclusion, since the data suggests that the increase does contribute to a more rapid out-diffusion of the iodide and bromide. The sensitivity to EDL thickness and ion-specific diffusivity will be investigated.

REFERENCES

Appelo, C.A.J., Wersin, P. (2007) Multicomponent diffusion modeling in clay systems with application to the diffusion of tritium, iodide, and sodium in Opalinus Clay. Environmental Science and Technology 41, 5002-5007.

Appelo, C.A.J., Vinsot, A., Mettler, S., Wechner, S. (2008) Obtaining the porewater composition of a clay rock by modeling the in- and out-diffusion of anions and cations from an in-situ experiment. Journal of Contaminant Hydrology 101, 67-76.

Birgersson, M., Karnland, O. (2009) Ion equilibrium between montmorillonite interlayer space and an external solution - Consequences for diffusional transport. Geochimica et Cosmochimica Acta 73, 1908-1923.

Birkholzer, J.T. (2012) Status of UFD Campaign International Activities in Disposal Research. Report prepared for U.S. Department of Energy Used Fuel Disposition Campaign, FCRD-UFD-2012-000295.

Birkholzer, J., Asahina, D., Chen, F., Gardner, P., Houseworth, J., Jove-Colon, C., Kersting, A., Nair, P., Nutt, M., Li, L., Liu, H.H., Painter, S., Reimus, P., Rutqvist, J., Steefel, C., Tynan, M., Wang, Y., Zavarin, M. (2013) An overview of US disposal research activities linked to international URLs. Proceedings of the 2013 International High-Level Radioactive Waste Management Conference (IHLRWM), April 28 – May 2, 2013, Albuquerque, New Mexico.

Corkum A.G., Martin C.D. (2007) The Mechanical Behaviour of Weak Mudstone (Opalinus Clay) at Low Stresses, International Journal of Rock Mechanics and Mining Sciences, 44, 196-209.

Davis, J., Rutqvist, J., Steefel, C., Tinnacher, R., Viarrasa, V., Zhen, L., Bourg, I., Liu, H.H., Birkholzer, J. (2013) Investigation of reactive transport and coupled THMC processes in the EBS: FY13 Report (FCRD-UFD-2013-000216), U.S. DOE Used Fuel Disposition Campaign.

Finsterle, S. (2007) iTOUGH2 User's Guide. Report LBNL-40040, Lawrence Berkeley National Laboratory, Berkeley, CA.

Garitte, B. (2012) HE-E experiment - In situ Heater Test, Presentation given at 1th DECOVALEX 2015 workshop, April 2012, Berkeley.

Garitte, B., Gens, A., Vaunat, J., Armand, G. (2013) Thermal Conductivity of Argillaceous Rocks: Determination Methodology Using In Situ Heating Tests. In Rock Mechanics and Rock Engineering DOI 10.1007/s00603-012-0335-x.

Gens, A., Garitte, B., Wileveau, Y. (2007) In situ Behaviour of a Stiff Layered Clay Subject to Thermal Loading: Observations and Interpretation, Geotechnique, 57, 207-228.

Gens, A., Sanchez, M., Guimaraes, L.D.N., Alonso, E.E., Lloret, A., Olivella, S., Villar, M.V., Huertas, F. (2009) A full-scale in situ heating test for high-level nuclear waste disposal: observations, analysis and interpretation. Geotechnique 59, 377–399.

Gonçalvès, J., Rousseau-Gueutin, P., Revil, A. (2007) Introducing interacting diffuse layers in TLM calculations: A reappraisal of the influence of the pore size on the swelling pressure and the osmotic efficiency of compacted bentonites. *J. Colloid Interface Sci.*, **316**, 92-99.

Graupner, B.J., Lee, C., Manepally, C., Pan, P., Rutqvist, J., Wang, W., Garitte, B. (2013) The Mont Terri HE-D Experiment as a Benchmark for the Simulation of Coupled THM Processes. Extended abstract for the European Association of Geoscientists & Engineers (EAGE) International Workshop Geomechanics & Energy, Lausanne, Switzerland, 26-28 November, 2013.

Itasca (2009) FLAC3D V4.0, Fast Lagrangian Analysis of Continua in 3 Dimensions, User's Guide. Itasca Consulting Group, Minneapolis, Minnesota.

Liu, H.H., Houseworth, J., Rutqvist, J., Zheng, L., Asahina, D., Li, L., Vilarrasa, V., Chen, F., Nakagawa, S., Finsterle, S., Doughty, C., Kneafsey, T., Birkholzer, J. (2013) Report on THMC modeling of the near field evolution of a generic clay repository: Model validation and demonstration. (FCRD-UFD-2013-000244), U.S. DOE Used Fuel Disposition Campaign.

Leroy, P., Revil, A. (2004) A triple-layer model of the surface electrochemical properties of clay minerals. Journal of Colloid and Interface Science 270, 371-380.

Leroy, P., Revil, A., Altmann, S., Tournassat, C. (2007) Modeling the composition of a pore water in a clay-rock geological formation (Callovo-Oxfordian, France). Geochimica et Cosmochimica Acta 71, 1087-1097.

Malusis M.A., Shackelford C.D. Explicit and implicit coupling during solute transport through clay membrane barriers. *J. Contam. Hydrol.*, **72**, 259-285 (2004).

Malusis M.A., Shackelford C.D., Olsen H.W. Flow and transport through clay membrane barriers. *Eng. Geol.*, **70**, 235-248 (2003).

Mammar N., Rosanne M., Prunet-Foch B., Thovert J.-F., Tevissen E., Adler P.M. Transport properties of compact clays. I. Conductivity and permeability. *J. Colloid Interface Sci.*, **240**, 498-508 (2001).

Nutt, M. (2011) Used Fuel Disposition Campaign Disposal Research and Development Roadmap (FCR&D-USED-2011-000065 REV0), U.S. DOE Used Fuel Disposition Campaign.

Olivella, S., Gens A. (2000). Vapour transport in low permeability unsaturated soils with capillary effects. Transport in porous Media 40: 219–241.

Pruess, K., Oldenburg, C.M., Moridis, G. (2011) TOUGH2 User's Guide, Version 2.1, LBNL-43134(revised), Lawrence Berkeley National Laboratory, Berkeley, California.

Rizzi, M., Seiphoori, A., Ferrari, A., Ceresetti, D., Laloui, L. (2011) Analysis of the Behaviour of the Granular MX-80 bentonite in THM-processes; Orders No 7'928 and 5'160; Swiss Federal Institute of Technology: Lausanne, 2011.

Rutqvist, J., Börgesson, L., Chijimatsu, M., Kobayashi, A., Nguyen, T.S., Jing, L., Noorishad, J., Tsang, C.-F. (2001a) Thermohydromechanics of partially saturated geological media – Governing equations and formulation of four finite element models. Int. J. Rock Mech. & Min. Sci. 38, 105-127.

Rutqvist J., Börgesson L., Chijimatsu M., Nguyen T. S., Jing L., Noorishad J., Tsang C.-F. (2001b) Coupled Thermo-hydro-mechanical Analysis of a Heater Test in Fractured Rock and Bentonite at Kamaishi Mine – Comparison of Field Results to Predictions of Four Finite Element Codes. Int. J. Rock Mech. & Min. Sci. 38, 129-142.

Rutqvist J., WuY.-S., Tsang C.-F., Bodvarsson G. (2002) A modeling approach for analysis of coupled multiphase fluid flow, heat transfer, and deformation in fractured porous rock. *International Journal of Rock Mechanics and Mining Sciences*, 39, 429-442.

Rutqvist J., Ijiri Y., Yamamoto H. (2011) Implementation of the Barcelona Basic Model into TOUGH–FLAC for simulations of the geomechanical behavior of unsaturated soils. *Computers &Geosciences*, 37, 751-762.

Rutqvist J., Zheng L., Chen F, Liu H.-H, Birkholzer J. (2013a) Modeling of Coupled Thermo-Hydro-Mechanical Processes with Links to Geochemistry Associated with Bentonite-Backfilled

Repository Tunnels in Clay Formations. *Rock Mechanics and Rock Engineering*, (In Press, January 2013).

Rutqvist, J., Chen F., Birkholzer J., Liu H.-H., Müller H., Garitte B., Vietor T. (2013b) Modeling of coupled thermo-hydro-mechanical processes at Mont Terri heater experiment in Opalinus Clay, using TOUGH-FLAC. Proceedings of the 2013 International High-Level Radioactive Conference (IHLRWM), April 28 – May 2, 2013.

Schoch, R.B., Han, J., Renaud, P. (2008) Transport phenomena in nanofluidics. Reviews of Modern Physics 80, 840-883.

Tournassat, C., Appelo, C.A.J. (2011) Modelling approaches for anion-exclusion in compacted Na-bentonite. Geochimica et Cosmochimica Acta 75, 3698-3710.

UFD (2012) Office of Used Fuel Disposition International Program — Strategic Plan (2013) April 2012, U.S. Department of Energy.

van Genuchten, M.T. (1980) A closed-form equation for predicting the hydraulic conductivity of unsaturated soils. Soil Sci Soc Am J 1980, 44, 892-898.

Villar, M.V. (2012) THM Cells for the HE-E Test: Setup and First Results; PEBS Report D2.2.7a. CIEMAT Technical Report CIEMAT/DMA/2G210/03/2012; Euratom 7th Framework Programme Project: PEBS: Madrid, Spain.

Wersin, P., Curti, E. Appelo, C.A.J. (2004) Modelling bentonite-water interactions at high solid/liquid ratios: swelling and diffuse double layer effects. Applied Clay Science 26, 249-257.

Wileveau, Y. (2005) THM behaviour of host rock: (HE-D experiment): Progress Report September 2003 – October 2004. Mont Terri Project, TR 2005-03.

Wileveau, Y., Rothfuchs, T. (2007) THM behaviour of host rock (HE-D) Experiment: Study of Thermal effects on Opalinus Clay. Mont Terri Project, TR 2006-01.